Early Cretaceous palaeogeographic evolution of the Coqen Basin in the Lhasa Terrane, southern Tibetan Plateau

Palaeogeography, Palaeoclimatology, Palaeoecology xxx (2017) xxx–xxx

Contents lists available at ScienceDirect

Palaeogeography, Palaeoclimatology, Palaeoecology

journal homepage: www.elsevier.com/locate/palaeo

Early Cretaceous palaeogeographic evolution of the Coqen Basin in the Lhasa Terrane, southern Tibetan Plateau

Gaoyuan Sun [a,b,*], Xiumian Hu [b], Hugh D. Sinclair [c]

[a] School of Earth Sciences and Engineering, Hohai University, Nanjing 211100, China
[b] State Key Laboratory for Mineral Deposits Research, School of Earth Sciences and Engineering, Nanjing University, Nanjing 210023, China
[c] School of GeoSciences, University of Edinburgh, Drummond Street, Edinburgh EH8 9XP, Scotland, UK

ARTICLE INFO

Article history:
Received 26 March 2017
Received in revised form 3 June 2017
Accepted 11 June 2017
Available online xxxx

Keywords:
Lower Cretaceous
Palaeogeography
Sedimentology
Provenance
Detrital zircon

ABSTRACT

The Lower Cretaceous sedimentary strata in the Lhasa Terrane record the palaeogeographic and tectonic history of the Tibetan Plateau prior to the India-Asia collision. The Lower Cretaceous strata in the Coqen Basin of the northern Lhasa subterrane include the Duoni and Langshan Formations. The Duoni Formation is composed of conglomerates, sandstones, siltstones and mudstones in the south deposited in a fluvial environment and quartzose-lithic sandstones, siltstones and mudstones in the north deposited in a shelf-coastal environment. The overlying Langshan Formation is characterized by abundant *Orbitolina*- and rudist-bearing wackestones and packstones, which were deposited on a low-energy carbonate ramp. The Langshan Formation in the Coqen Basin was deposited between ~119–115 Ma and ~98 Ma based on its large benthic foraminiferal assemblages. Age constraints based on the interbedded tuff and conformably overlying Langshan Formation indicate that the Duoni Formation was deposited between ~123 and 115 Ma. Sandstone detrital modal compositions further indicate that the Duoni Formation was primarily derived from magmatic arc and recycled orogen sources. Detrital zircons from the Duoni Formation yield a primary age population of 160–110 Ma (peaking at ~130 Ma), with negative $\varepsilon_{Hf}(t)$ values (−18.7 to −2.7), and additional age ranges of 550–500, 1200–900, and 1600–1500 Ma, thereby indicating that the Zenong volcanic rocks and Palaeozoic sedimentary bedrocks in the northern Lhasa subterrane are the most likely sources. The palaeogeography of the northern Lhasa subterrane can be approximately described in two stages. During the Aptian (~123–115 Ma), with the eruption of the Zenong volcanic rocks, the Duoni Formation accumulated in fluvial and shelf-coastal environments and was sourced from the Zenong volcanic rocks and basement rocks from the southern region of the northern Lhasa subterrane. The enhanced magmatic activities in the northern Lhasa subterrane may have influenced the Duoni Formation deposition. During the Late Aptian-Early Cenomanian (~115–98 Ma), a north-south transgression occurred, causing the majority of the northern Lhasa region to be dominated by shallow-marine limestones of the Langshan Formation.

1. Introduction

The Lhasa Terrane was the last to accrete onto the southern margin of the Asian plate in the Late Jurassic-Early Cretaceous (Kapp et al., 2007a; Zhu et al., 2013, 2016); thus, it records the early tectonic history of the Tibetan Plateau prior to the India-Asia collision (Dewey et al., 1988; Yin and Harrison, 2000). During the Cretaceous, the Lhasa Terrane was influenced by the Lhasa-Qiangtang collision to the north and subduction of the Neo-Tethyan oceanic lithosphere to the south (England and Searle, 1986; Murphy et al., 1997; Kapp et al., 2007b; Leier et al., 2007a, 2007b). The tectonic evolution of the Lhasa Terrane in the Early Cretaceous is unknown. An Early Cretaceous palaeogeographic reconstruction of the Lhasa Terrane would help to understand its basin evolution and the southern Asia margin tectonic framework prior to the India-Asia collision. Several published studies have analysed the sedimentology and provenance of the Cretaceous basins on the northern Lhasa subterrane (Leier et al., 2007a, 2007b; Zhang et al., 2004, 2011, 2012). However, the Early Cretaceous palaeogeography of the Lhasa Terrane remains under intense debate. For example, Murphy et al. (1997) suggested that the southern Tibetan Plateau (Lhasa Terrane) has been uplifted by approximately 3–4 km since the Early Cretaceous due to the Lhasa-Qiangtang collision to the north. However, Zhang et al. (2004, 2012) inferred that the Lhasa Terrane remained at approximately sea level until the Early Cenomanian and that its geography was primarily controlled by the subducted Neo-Tethyan oceanic lithosphere to the south.

The Coqen Basin, which is located in the northern Lhasa subterrane and is bounded by the Gangdese magmatic arc to the south and

* Corresponding author at: School of Earth Sciences and Engineering, Hohai University, Nanjing 211100, China.
E-mail address: sungy@hhu.edu.cn (G. Sun).

http://dx.doi.org/10.1016/j.palaeo.2017.06.006
0031-0182/

Bangong-Nujiang suture to the north, is an ideal site to document the Early Cretaceous history of this region. The Lower Cretaceous deposits in the Coqen Basin include the Duoni Formation clastic rocks and Langshan Formation limestones. To test the palaeogeographic evolution of the Lhasa Terrane, this study presents new data on the sedimentology, stratigraphy, and detrital zircon geochronology of the Lower Cretaceous strata in the Coqen Basin. These new results, combined with previously published data, provide new information to build a chronostratigraphic framework of the Lhasa Terrane during the Early Cretaceous and to detect the sedimentary sources of the clastic rocks, thereby allowing its palaeogeography to be reconstructed. We believe that relative to the other sedimentary basins on the Lhasa Terrane, the magmatic activities and north-south transgression had significant influences on the Early Cretaceous deposition.

2. Geological setting

The Tibetan Plateau comprises, from north to south, the Songpan-Ganzi complex, the Qiangtang Terrane, and the Lhasa Terrane, which are separated by the Jinsa and Bangong-Nujiang sutures (Fig. 1A, Yin and Harrison, 2000). The Lhasa Terrane is separated from the Tethyan Himalaya to the south by the Yarlung-Zangbo suture zone, which represents the Palaeocene India-Asia collisional suture zone (Fig. 1A, Yin and Harrison, 2000; Zhu et al., 2013; DeCelles et al., 2014; Hu et al., 2015, 2016, 2017). The Lhasa Terrane collided with the Qiangtang Terrane along the Bangong-Nujiang suture zone in the Late Jurassic to Early Cretaceous (Dewey et al., 1988; Kapp et al., 2007b; Zhu et al., 2013, 2016).

Traditionally, the Lhasa Terrane is divided into two domains by the Luobadui-Milashan Fault (LMF), a southern and a northern subterrane (Fig. 1A, Burg et al., 1983; England and Searle, 1986; Searle et al., 1987; Yin and Harrison, 2000; Pan et al., 2004). The southern Lhasa subterrane is primarily composed of the Gangdese magmatic arc and the Xigaze forearc basin. The Late Triassic-Early Cenozoic Gangdese batholiths and Cenozoic Linzizong volcanic rocks are the primary components of the Gangdese magmatic arc (Chu et al., 2006; Mo et al., 2007, 2008; Wen et al., 2008; Ji et al., 2009; Lee et al., 2009; Zhu et al., 2011a, 2015), which is related to the northward subduction of Neo-Tethyan oceanic lithosphere beneath the Lhasa Terrane and the subsequent India-Asia collision (Yin and Harrison, 2000; Ding et al., 2003; Ji et al., 2009). The Xigaze forearc basin, which is located on the southern margin of the Gangdese magmatic arc, is characterized by thick sequences of Albian–Campanian deep-water turbidites followed by Campanian-Maastrichitian shallow-water deposits (Dürr, 1996; Wang and Liu, 1999; Wang et al., 2012; An et al., 2014; Orme et al., 2014; Orme and Laskowaki, 2016). The Gangdese magmatic arc was a significant sediment source for the Xigaze forearc basin, in addition to the northern Lhasa subterrane that also sourced detritus materials (Wu et al., 2010; An et al., 2014).

In the northern Lhasa subterrane, there are widespread Cretaceous magmatic rocks that are characterized as the Zenong volcanic rocks (Zhu et al., 2008, 2009, 2011a). Successions of Carboniferous metasedimentary rocks, Permian limestone, and Jurassic siliciclastic rocks are exposed in the northern Lhasa subterrane (Leeder et al., 1988; Yin et al., 1988). Thick Cretaceous strata are also preserved in the sedimentary basins in the northern Lhasa subterrane; these include the Lower Cretaceous Duoni Formation clastic rocks, the Langshan Formation limestones and the Upper Cretaceous continental fluvial conglomerates and sandstones (Zhang et al., 2004, 2011, 2012; He et al., 2007; Leier et al., 2007a, 2007b; Volkmer et al., 2007; DeCelles et al., 2007).

The study area (i.e., the Coqen Basin) is located in the northern Lhasa subterrane. Geographically, it is located between the town of Coqen and the village of Dong Co; geologically, it is connected to the Gangdese magmatic arc to the south and bounded by the Bangong-Nujiang suture zone to the north (Fig. 1A). Lower Cretaceous volcanic and sedimentary rocks are well exposed in the Coqen Basin. The Lower Cretaceous Zenong volcanic rocks are also widespread throughout the southern part of the Coqen Basin. Recently published zircon U-Pb ages from the

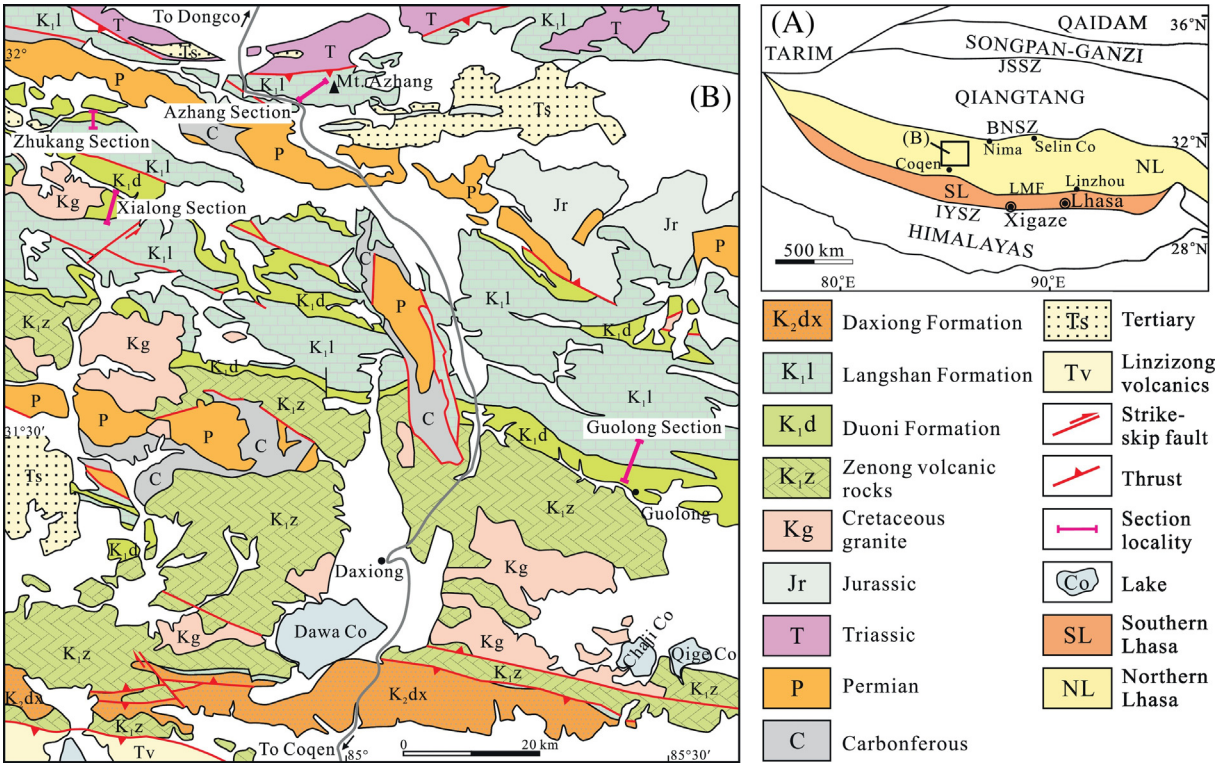

Fig. 1. (A) Simplified tectonic map of the Tibetan Plateau and adjacent regions (Pan et al., 2004). JSSZ—Jinsha suture zone; BNSZ—Bangong-Nujiang suture zone; IYSZ—Indus-Yarlung suture zone; LMF—Luobadui–Milashan Fault; NL—Northern Lhasa subterrane; SL—Southern Lhasa subterrane. (B) Simplified geological map of the Coqen Basin, showing the studied sections, modified from the 1:250,000-scale regional geological survey in Tibet (Coqen area) (Liu et al., 2004).

Please cite this article as: Sun, G., et al., Early Cretaceous palaeogeographic evolution of the Coqen Basin in the Lhasa Terrane, southern Tibetan Plateau, Palaeogeogr. Palaeoclimatol. Palaeoecol. (2017), http://dx.doi.org/10.1016/j.palaeo.2017.06.006

Coqen area reveal that the Zenong volcanic rocks erupted ca. 130–107 Ma (Zhu et al., 2008, 2009, 2011a). The Duoni Formation overlies the Zenong volcanic rocks and consists of volcaniclastic sandstones, conglomerates, siltstones and mudstones (Liu et al., 2004). The Langshan Formation, which conformably overlies the Duoni Formation, consists of rudist- and foraminifera-bearing limestones (Leeder et al., 1988; Leier et al., 2007a; Zhang et al., 2012).

3. Methods

3.1. Sedimentology and palaeocurrent data

We measured detailed stratigraphic sections at 4 different locations (Fig. 1B). Through the investigation of lithofacies associations and sedimentary features, the probable depositional environments and sedimentary microfacies of these sections were determined. Palaeocurrent data were measured in the field from cross stratification. All original measured data were corrected to the horizontal by standard stereonet techniques, in which the average trough-axis orientation of each point was measured and determined statistically on a stereographic plot of 15–20 trough limbs (method I of DeCelles et al., 1983).

3.2. Sandstone petrography

A total of 55 sandstone thin sections from the Duoni Formation were generated and analysed by modal framework-grain triplets. Approximately 400 grains were counted in a random area of each section using an appropriate grid based on the grain size (i.e., the Gazzi-Dickinson method of Ingersoll et al., 1984).

3.3. In situ zircon U-Pb dating and Hf isotopes

Zircons were separated from the tuff horizons and medium-grained sandstones of the Duoni and Langshan Formations. Zircon U-Pb dating was conducted at the State Key Laboratory for Mineral Deposits Research, Nanjing University, China. U-Pb ages were obtained by laser ablation inductively-coupled plasma mass spectrometry (LA-ICP-MS) following the method described by Jackson et al. (2004). In this study, $^{206}Pb/^{238}U$ ages were used for zircons yielding ages of <1000 Ma and $^{207}Pb/^{206}Pb$ ages were used for zircons yielding ages >1000 Ma. Measured ages with >10% discordance were excluded in this study. The primary Pb isotopic results were calculated by GLITTER 4.4 (Van Achterbergh et al., 2001) and common Pb corrections were conducted following the method of Andersen (2002). Detrital zircon age probabilities and weighted mean age calculations were performed by the Isoplot/Ex program (version 2.49) of Ludwig, 2001. The errors are within 1σ and 2σ for individual zircon ages and weighted mean ages, respectively.

Some zircons measured for their U-Pb ages were also measured for their in situ Hf isotopic compositions at the State Key Laboratory for Mineral Deposits Research, Nanjing University, China, using a Thermo Scientific Neptune Plus MC-ICP-MS coupled to a New Wave UP193 solid-state laser ablation (LA) system. The laser ablation beam has a diameter of 35 μm and a laser repetition rate of 8 Hz. Measurements of each grain were collected 200 times per minute. To calculate the results, we used a ^{176}Lu decay constant of 1.867×10^{-11} a^{-1} (Soderlund et al., 2004). The calculations of $\varepsilon_{Hf}(t)$ and Hf crust model ages (T^{C}_{DM}) were performed using the methods of Bouvier et al. (2008) and Griffin et al. (2002), respectively.

The youngest measured detrital zircon ages are commonly used to constrain the maximum depositional ages of stratigraphic units. The calculation are of different methods (Table 1, the detailed methods can be referred to Dickinson and Gehrels, 2009) and the YC1σ(2+) age is applied by this study. A comparison of the age distributions of detrital and potential source area zircons reveals that they have remarkably similar age spectra (i.e., similar peaks and troughs). In addition, zircon Hf isotopic data record distinctive crustal histories, which also reveal important information about the sedimentary provenance and tectonic setting of the basin in which they accumulated (Cawood et al., 2012).

4. Sedimentology

Four sections in the field were studied in detail and underwent sedimentary facies analysis. The locations of these sections are shown in Fig. 1B. The sedimentary characteristics of the Lower Cretaceous strata, which reflect the depositional processes in the study area, can be observed in the following several lithofacies.

4.1. Duoni Formation (southern region of the Coqen Basin)

4.1.1. Conglomerate and coarse-grained pebbly sandstone lithofacies association

The conglomerate and coarse-grained pebbly sandstone lithofacies association is very common in the bottom of the Guolong section (Fig. 2). This lithofacies association consists of an approximately 3–5 m thick series of upward-fining packages. The lower part of the package is generally composed of ~0.5–1 m thick conglomerate beds. The conglomerate beds display imbricated clasts, subhorizontal stratification, and trough and planar cross-stratifications, with wedge and lenticular shapes and basal scour surfaces (Fig. 4D). The clasts are mainly composed of volcanic rocks, quartz sandstones and limestones, all of which are poorly sorted and well rounded. The average clast size is ~5 cm in diameter, with a maximum clast size of ~10 cm. The conglomerate beds are dominated by a matrix-supported texture with a coarse-grained sandstone matrix. The conglomerate beds commonly fine upwards into the middle part of the coarse-grained pebbly sandstones, which generally exhibit trough and planar cross-stratifications and plane-parallel laminations. An upper section of very thinly bedded, fine-grained sandstones and mudstones overlies the coarse-grained sandstone beds. Palaeocurrent data measured from trough and planar cross-stratifications indicate a roughly northward palaeoflow direction.

This lithofacies association is interpreted to reflect a series of gravelly fluvial channels within meandering rivers (Miall, 1978, 1996; Diemer and Belt, 1991). The upward-fining sequences within the sandstone

Table 1
Young detrital zircon U-Pb ages of the sandstones from the Duoni Formation.

Section	Sample	Zircon grains	Percentage of the Mesozoic zircons	YSG(Ma)	**YC1σ(2+)**	YC2σ(3+)	YPP	YDZ
				Ma	**Ma**	Ma	Ma	Ma
Guolong	13GL98	108	46.3%	109 ± 4	**113.9 ± 1.8 (n = 13)**	116.1 ± 2.0 (n = 20)	112.2	107.7 + 3.1/−8.4
	13GL105	105	60.0%	103 ± 6	**106.7 ± 1.5 (n = 13)**	107.7 ± 1.6 (n = 17)	105.5	102.5 + 2.2/−13
	13GL140	106	23.6%	105 ± 2	**111.1 ± 2.5 (n = 12)**	114.4 ± 2.6 (n = 19)	113.9	104.4 + 3.1/−4.1
Xialong	12ZN02	73	54.8%	113 ± 4	**122.8 ± 1.8 (n = 13)**	125.3 ± 1.6 (n = 24)	128.9	112.9 + 5.9/−8.9
	12ZN06	102	29.4%	118 ± 2	**123.5 ± 2.5 (n = 13)**	126.5 ± 2.2 (n = 23)	119.7	116.5 + 3.0/−3.5
	12XL109	115	34.8%	114 ± 3	**119.1 ± 2.0 (n = 7)**	126.0 ± 2.5 (n = 22)	119.4	113.7 + 3.9/−6.3

YSG—Youngest single detrital; YC1σ(2+)—Weighted mean age of two or more youngest grain ages overlapping in age at 1σ; YC2σ(3+)—Weighted mean age of two or more youngest grain ages overlapping in age at 2σ; YPP—Youngest graphical detrital zircon age peak on an age-probability; YDZ—Age calculated by the "youngest detrital zircon" routine of Isoplot. Refer to Dickinson and Gehrels (2009).

Please cite this article as: Sun, G., et al., Early Cretaceous palaeogeographic evolution of the Coqen Basin in the Lhasa Terrane, southern Tibetan Plateau, Palaeogeogr. Palaeoclimatol. Palaeoecol. (2017), http://dx.doi.org/10.1016/j.palaeo.2017.06.006

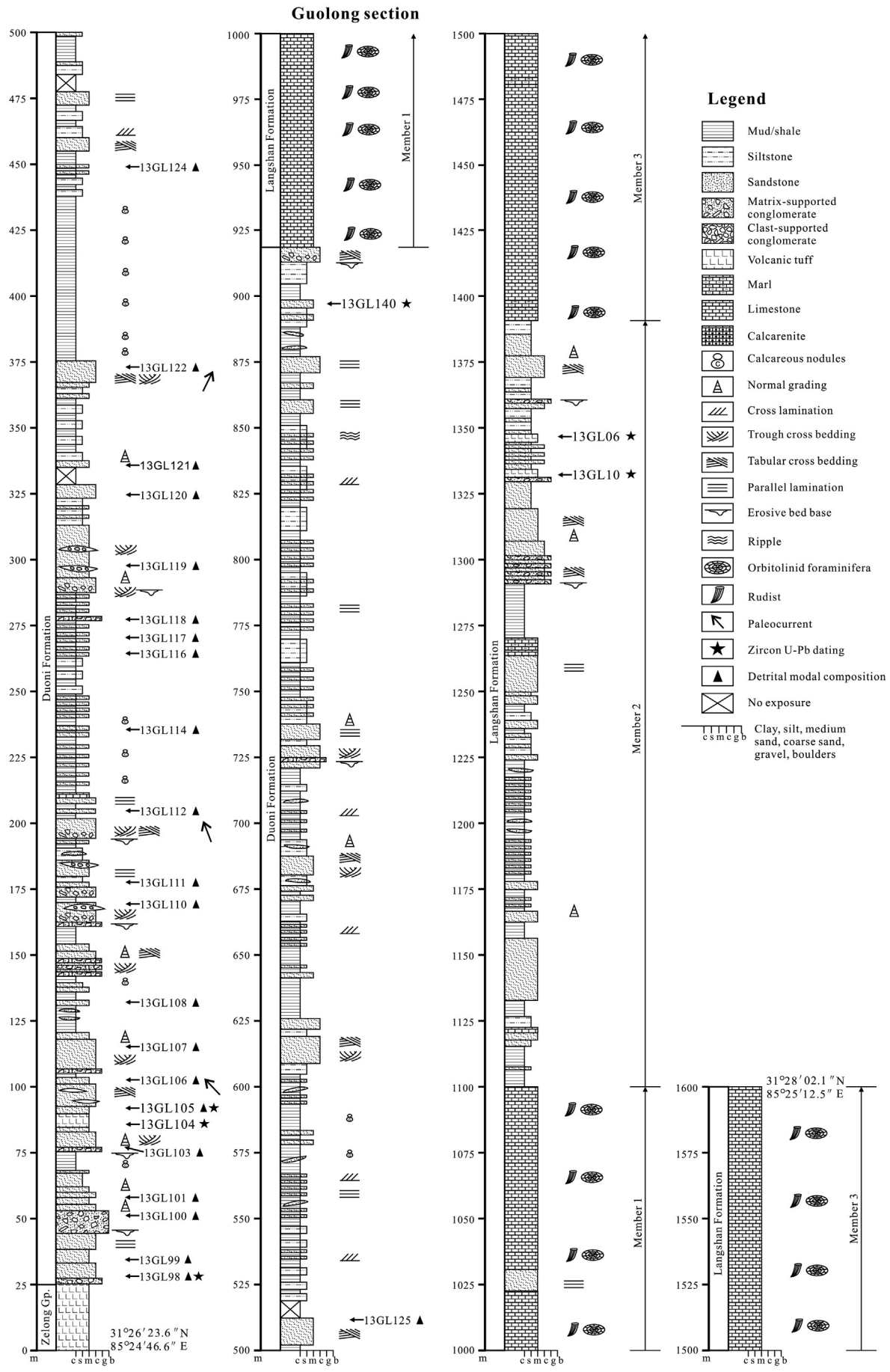

Please cite this article as: Sun, G., et al., Early Cretaceous palaeogeographic evolution of the Coqen Basin in the Lhasa Terrane, southern Tibetan Plateau, Palaeogeogr. Palaeoclimatol. Palaeoecol. (2017), http://dx.doi.org/10.1016/j.palaeo.2017.06.006

units of this lithofacies association are most common in river channels, and its cross-stratifications record the shifts of sand bar sets (Miall, 1996).

4.1.2. Medium- to coarse-grained sandstone lithofacies association

This lithofacies association is mainly composed of grey, medium- to coarse-grained lithic sandstone beds, which record a gradual transition from the underlying conglomerate or coarse-grained pebbly sandstone lithofacies. Upward-fining packages are well developed in this lithofacies, and pebbly coarse sandstone beds (~10–40 cm in thickness) are present in the lower unit. Individual packages are separated from each other by scour planes, in which the pebbly sandstone clasts appear to have been recycled from the underlying siltstone or mudstone beds. These packages comprise laterally extensive, lithic- or quartz-rich sandstone beds, with a thickness of approximately 4 m. Occasionally, thin (<1 m thick) lenticular, fine conglomerate beds or pebbly, very coarse sandstone beds are developed. Planar and trough cross-stratifications are well developed in the sandstone beds (Fig. 4E). Very thin (<0.2 m thick) red or purple mudstone and siltstone beds at the top of the packages exhibit plane-parallel laminations and current ripples, with few plant fossils. The cross-stratifications of this lithofacies indicate a roughly northward palaeocurrent direction.

The thick sandstone bodies are interpreted to have been deposited in fluvial channels (Diemer and Belt, 1991; Bridge, 2009). Their trough and planar cross-stratifications record the migration of subaqueous three- and two-dimensional dunes within these palaeochannels (Allen, 1964). The thin mudstone/siltstone intervals interstratified between the sandstone beds are interpreted to have been deposited in an overbank floodplain setting (Cant and Walker, 1978).

4.1.3. Fine sandstone interstratified with siltstone/mudstone lithofacies association

This lithofacies association is well developed in the middle part of the Guolong section, with a total thickness of ~200 m. The purple and red fine sandstone beds (which are approximately 0.5 to 1 m thick) are interstratified with grey or red mudstone or siltstone beds of similar thickness. There are also some horizontal beddings and current and climbing ripples developed in the fine sandstone beds. In addition, thin (<0.5 m thick) sheet-shaped, medium-grained sandstone beds are occasionally found interbedded in the fine sandstones and record small-scale cross-stratifications. The mottled mudstone is commonly laminated and contains very fine-grained and thin (centimetre-scale and laterally pinched out) sandstone beds. Many $CaCO_3$ nodules appear in the red mudstone beds.

This lithofacies association is interpreted to have been deposited on the overbank of a floodplain. The few thinly bedded (sheet-like) medium-grained sandstones interstratified in the fine sandstones are interpreted to have been formed by crevasse-splays during floods (Leier et al., 2007a). The mudstone beds with $CaCO_3$ nodules represent calcretes that are typical of floodplains with fluctuating groundwater levels (Mack et al., 1993; Kraus, 1999).

4.1.4. Massive mudstone lithofacies association

Massive red and green mudstone beds occur in the middle to upper parts of the Guolong section. The thickness of each bed is commonly between 10 and 20 m and increases moving upward in the section. A few thin (~2 m thick) and lenticular medium-grained sandstone beds with minor current ripples are also developed in the massive mudstones. Green mudstone beds tend to be thicker (up to >20 m thick) and are more abundant in the upper part of the section. $CaCO_3$ nodules and plant fragments are quite common in the massive mudstone beds.

This massive mudstone lithofacies is interpreted to have been deposited in the relatively low regions of the floodplains under low-energy hydrodynamic conditions (Miall, 1978, 1996; Diemer and Belt, 1991; Bridge, 2009). Meanwhile, the abundance of $CaCO_3$ nodules and plant fragments in the mudstone units indicates that these deposits experienced occasional aridification (Mack et al., 1993; Kraus, 1999).

4.2. Duoni Formation (northern region of the Coqen Basin)

4.2.1. Quartz sandstone lithofacies association

This lithofacies association is mostly composed of the grey quartz sandstones and volcaniclastic quartz sandstones exposed in the Zhukang and Xialong sections, which are ~250 m thick (Fig. 3). The sandstone beds are generally ~3 m thick and are composed of quartz-rich, medium-grained sandstones, which contain planar and parallel cross-stratifications, current ripples and symmetrical ripples (Fig. 4G). There are also thin (~0.1 m thick) layers of conglomerate and pebbly, very coarse-grained sandstone below the main sandstone bodies, in which most clasts are recycled from the underlying strata. Within the entire sandstone package, the sandstone tends to be upward-coarsening. Some bivalve fossils have been found in the sandstone beds (Fig. 4F).

This lithofacies has a similar texture and composition as a mature quartz sandstone, which is believed to accumulate in a nearshore, wave-influenced setting (van Wagoner et al., 1988). In this environment, unstable feldspars and lithic fragments are removed. The upward-coarsening sequence generally represents the regression of the shoreline (van Wagoner et al., 1988; Van Wagoner et al., 1990; Posamentier and Allen, 1999).

4.2.2. Fine-grained sandstone and mudstone lithofacies association

The fine-grained sandstone lithofacies association is quite common in the Zhukang and Xialong sections and is mainly composed of dark grey laminated fine-grained sandstones and siltstones. Generally, these sandstone beds are interbedded with thin layers of laminated mudstones. The sandstone beds are typically an average of ~1 m thick (but vary in thickness from 0.1 m to 2 m) and generally display sharp contacts with underlying mudstones. Some bivalve fragments have been found in these sandstone beds. Plane-parallel laminations and oscillatory wave ripples are also common in the fine-grained sandstone beds (Fig. 4G). The mudstone beds are commonly ~1.5 m thick and contain horizontal or subhorizontal burrows. In some regions, the medium-grained sandstones are interbedded with black mudstones, which are approximately ~0.2 m thick. These sandstone beds generally have lenticular basal contacts and laterally extend to lengths of up to ~6–10 m.

This lithofacies association is interpreted to have been deposited in a shallow-marine shelf environment (Walker and Plint, 1992; Orton and Reading, 1993; Johnson and Baldwin, 1996). Fine-grained sandstones are mostly controlled by waves in shallow-marine domains, where they can receive materials from the land. The mudstone in this lithofacies association is interpreted to reflect quiet water deposits under the normal wave base, where the sediments are mostly derived from materials suspended in water. The medium-grained sandstone beds with lenticular basal contacts are interpreted to represent the accumulation of deposits from storm events below the normal wave base (Kreisa, 1981; Myrow and Southard, 1991).

4.2.3. Massive mudstone/siltstone lithofacies association

This lithofacies association is a well-exposed and at least ~450-m-thick section of the Zhukang section that comprises a series of massive dark mudstone or siltstone beds, each of which has an average thickness

Fig. 2. Lithological columns and sedimentary symbols of the Guolong section in the southern region of the Coqen Basin; the Latitude and longitude data correspond to the start and end point of the section; sample locations for zircon analyses and modal compositions are indicated by triangles and stars, respectively.

Please cite this article as: Sun, G., et al., Early Cretaceous palaeogeographic evolution of the Coqen Basin in the Lhasa Terrane, southern Tibetan Plateau, Palaeogeogr. Palaeoclimatol. Palaeoecol. (2017), http://dx.doi.org/10.1016/j.palaeo.2017.06.006

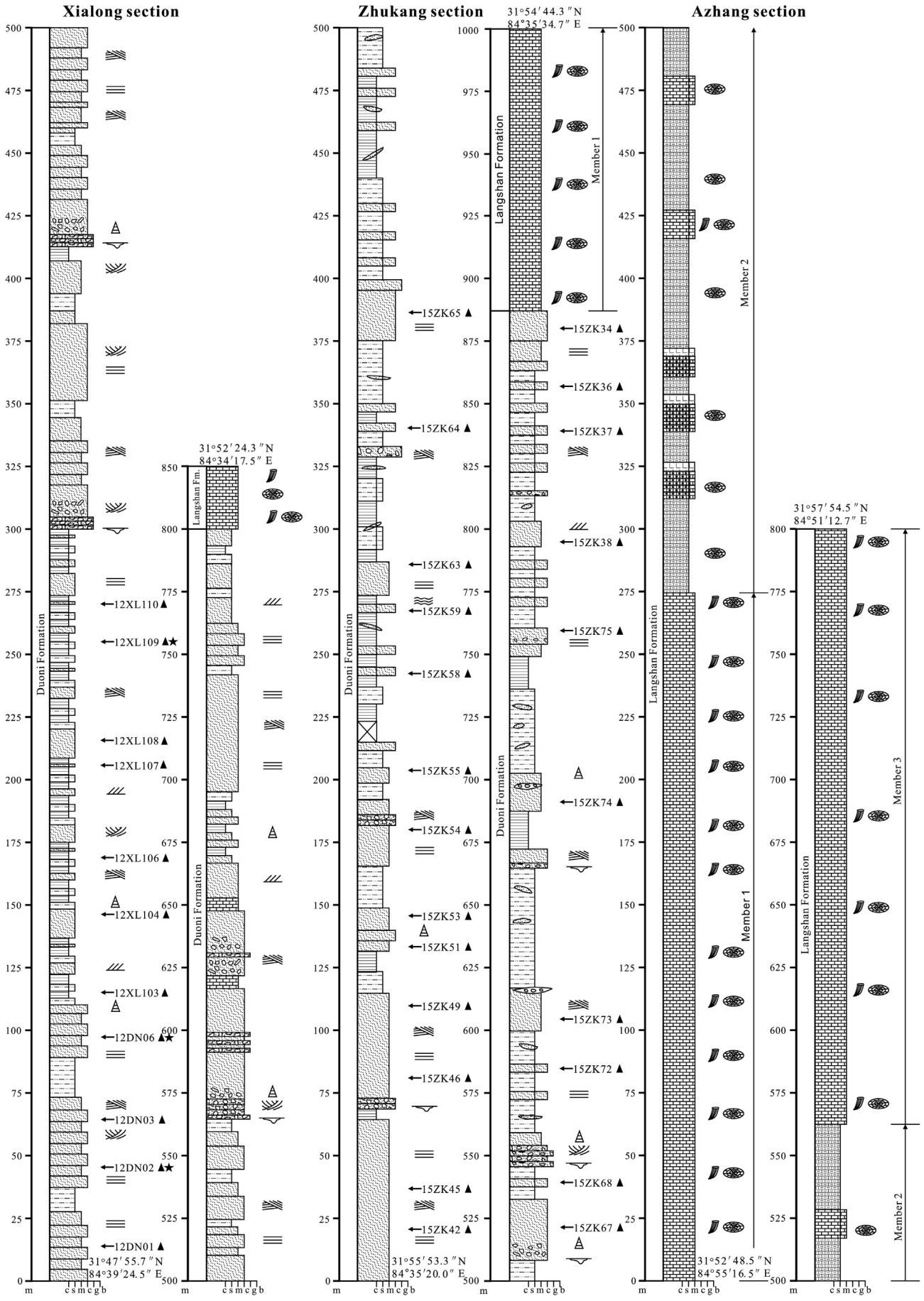

Please cite this article as: Sun, G., et al., Early Cretaceous palaeogeographic evolution of the Coqen Basin in the Lhasa Terrane, southern Tibetan Plateau, Palaeogeogr. Palaeoclimatol. Palaeoecol. (2017), http://dx.doi.org/10.1016/j.palaeo.2017.06.006

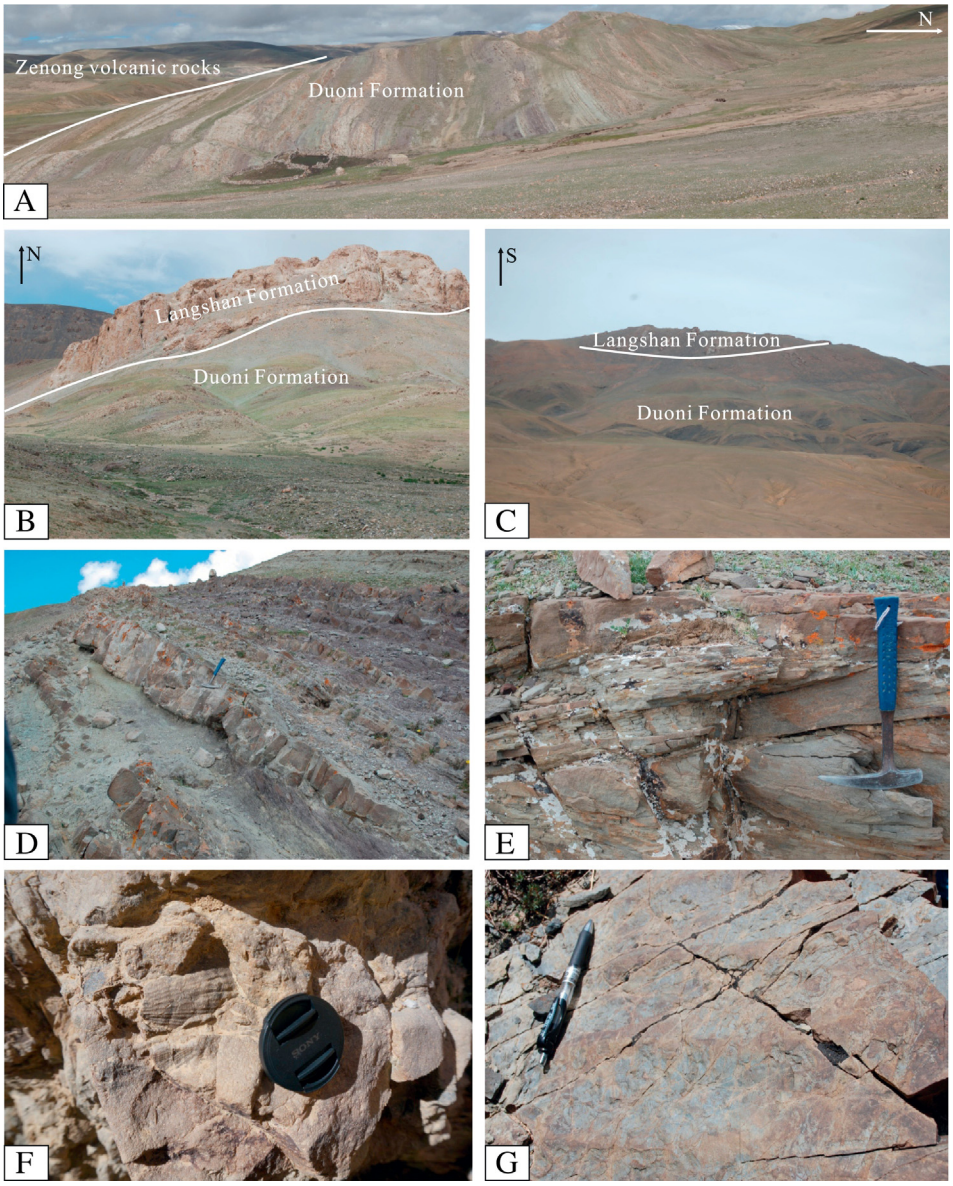

Fig. 4. (A) Panoramic photograph for Guolong section, showing the lower parts of the Duoni Formation and the relationship with the underlying strata. (B) Panoramic photograph for Guolong section, showing the upper part of the Duoni Formation and the relationship with the overlying Langshan Formation. (C) Panoramic photograph for Azhang section, showing the Langshan Formation (D) Coarse and pebbly sandstone beds with wedge and lenticular shapes and the basal scour surfaces (Guolong section). Hammer is 41 cm long. (E) Medium-coarse sandstone beds with the planar cross-stratification (Guolong section). Hammer is 41 cm long. (F) shell-bearing sandstone beds in Duoni Formation of the Zhukang section. (G) Ripples in the Duoni Formation. Pen is 15 cm long.

of ~5 m. In this section, there are few recorded sedimentary textures, but some plant and bivalve fragments have been observed. Very thin coal lines are found in the upper part of the section. In the upper part of this lithofacies, some olistostromal sandstone and conglomerate blocks, approximately 0.5 m × 1.2 m in size, are exposed. This sandstone is medium-grained and nodule-shaped with a sandstone shell, whereas the clasts of the conglomerate are mostly well-rounded sandstone clasts that are approximately ~5 cm × 8 cm in size.

The deposits containing plant fossils and coal lines in this lithofacies association are interpreted to have been deposited in a low-energy lagoon in the marginal sea with some terrigenous materials (Kirschbaum, 1989). The olistostromal sandstone and conglomerate blocks are interpreted to have deposited under the process of gravity sliding (Festa et al., 2010).

4.3. Langshan Formation

The Langshan Formation is well preserved in the Coqen Basin and conformably overlies the Duoni Formation. In the study area, the Langshan Formation is approximately 700–800 m thick and can be divided into three members (Fig. 2 and 3): Member 1 (~180–275 m) and Member 3 (~210 m) are composed of wackestones and packstones, which contain abundant large benthic foraminifera and rudists (Fig. 5D

Fig. 3. Lithological columns and sedimentary symbols of the Xialong, Zhukang and Azhang sections in the northern region of the Coqen Basin; the Latitude and longitude data correspond to the start and end point of the every sections; sample locations for zircon analyses and modal compositions are indicated by triangles and stars, respectively.

Please cite this article as: Sun, G., et al., Early Cretaceous palaeogeographic evolution of the Coqen Basin in the Lhasa Terrane, southern Tibetan Plateau, Palaeogeogr. Palaeoclimatol. Palaeoecol. (2017), http://dx.doi.org/10.1016/j.palaeo.2017.06.006

and E), whereas Member 2, which is located in the southern region of the study area (i.e., the Guolong section) includes medium-grained sandstones and mudstones. In the north part of the Coqen Basin (i.e., the Azhang section), Member 2 comprises marls interbedded with calcarenites.

The lithofacies associations of Members 1 and 3 mainly comprise thick-bedded to massive grey-yellow wackestones and minor packstones (which increase up-section). In the wackestones, rudists make up ~10% of the rock and large benthic foraminifera (mainly *Orbitolina*) account for ~15%. Marl represents the main component of the matrix. In the packstones, rudists and large benthic foraminifera (mainly *Orbitolina*) dominate the limestone and comprise 15% and 20%, respectively, of its composition. In addition to a micrite matrix, some of the packstones feature cements made of mostly calcites and recrystallized calcites. In addition, small planktonic foraminifera, algae and bivalve fragments are also present, but only occupy less than ~5% of the total components. This lithofacies association suggests that Member 1 and Member 3 of the Langshan Formation were deposited on a carbonate ramp in a shallow lagoonal environment near an open marine setting with good water circulation (Wray, 1977; Reiss and Hottinger, 1984; Flügel, 2004).

The lithofacies association of Member 2 in the Guolong section (located in the southern region of the Coqen Basin, Fig. 2) is composed of medium-grained volcaniclastic sandstones interbedded with mudstones and siltstones. This lithofacies association is similar to the "medium- to coarse-grained sandstone lithofacies association" in the Duoni Formation. The sandstone beds containing abundant cross-stratification beddings are interpreted to have been deposited in the channels of a fluvial system. The siltstone and mudstone beds are interpreted to have been deposited in the overbank of a floodplain.

The lithofacies association of Member 2 in the Azhang section (located in the northern region of the Coqen Basin, Fig. 3) is dominated by massive greenish marl interstratified with very thin (~5–10 cm thick) wackestone and calcarenite beds (in which the quantity of the beds decreases up-section). The interbedded wackestone and calcarenite are mainly composed of 15% large benthic foraminifera (mainly *Orbitolina*) and 5% well-sorted terrigenous clasts. The environment of this lithofacies is interpreted to be a low-energy lagoon setting (Reiss and Hottinger, 1984; Flügel, 2004).

5. Age constraints

5.1. Langshan Formation

In this study, we combine the zircon U-Pb dating results of interstratified tuff horizons and micro-palaeontological analysis of limestones to determine a credible depositional age for the Langshan Formation. Large, abundant benthic foraminifera are observed in the Guolong and Azhang sections, within which seven biozones were identified (for more details about the biozone divisions, refer to BouDagher-Fadel et al., 2017). In detail, the presence of *Dictyoconus cuvillieri*, *Mesorbitolina libanica*, *Conicorbitolina zhangia*, *Conicorbitolina cuvillieri*, and *Pseudocyclammina vasconica* in the Guolong section (within the southern region of the Coqen Basin) implies that the Langshan Formation deposition had been ongoing since ~115 Ma and ceased at ~98 Ma. Two tuffs (Samples 13GL06 and 13GL10, refer to Fig. 2) from Member 2 of the Langshan Formation in the Guolong section yield zircon U-Pb ages of 112.5 ± 1.7 Ma (n = 21, MSWD = 1.6) and 110.3 ± 1.0 Ma (n = 37, MSWD = 1.2) (Fig. 8, Appendix A), respectively. These zircon ages coincide with those of the LBF biozones (TLK1c, 113–110 Ma, see BouDagher-Fadel et al., 2017). Similarly, the presence of *Mesorbitolina libanica*, *Mesorbitolina delicata*, *Palaeodictyoconus arabicus*, *Conicorbitolina zhangia*, *Cuneolina parva*, and *Orbitolina sefini* in the Azhang section (in the northern Coqen Basin) indicates that the Langshan Formation age in this location ranges between ~119 Ma and ~98 Ma. Because the base of the Langshan Formation is absent in the Azhang section in the field, it is suspected that in the northern Coqen Basin, the Langshan Formation deposition began at approximately 119 Ma or earlier. Collectively, the Langshan Formation deposition in the Coqen Basin began earlier in its northern region (~119 Ma in the Azhang section) before extending to the south (~115 Ma in the Guolong section). By approximately 98 Ma, the Langshan limestone deposition had ceased.

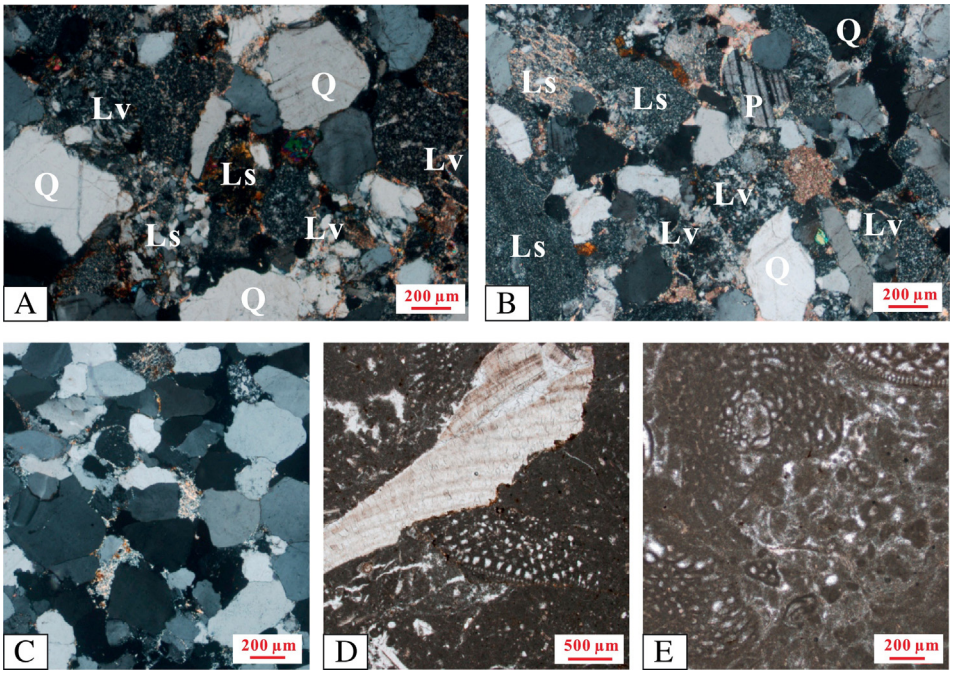

Fig. 5. Petrography of the Duoni and Langshan Formations. (A) Lithic sandstone (Sample 13GL105, Guolong section), showing volcanic and sedimentary fragments. (B) Lithic sandstone (Sample 13GL98, Guolong section), showing volcanic and sedimentary fragments. (C) Quartz-rich sandstone (Sample 13ZK75, Zhukang section). (D) rudist-fragment rich limestone from the Langshan Formation (Sample 12LS43, Azhang section). (E) *Orbitolina*-bearing limestone from the Langshan Formation (Sample 12LS29, Azhang section).

Please cite this article as: Sun, G., et al., Early Cretaceous palaeogeographic evolution of the Coqen Basin in the Lhasa Terrane, southern Tibetan Plateau, Palaeogeogr. Palaeoclimatol. Palaeoecol. (2017), http://dx.doi.org/10.1016/j.palaeo.2017.06.006

5.2. Duoni Formation

The Duoni Formation is primarily composed of medium-grained sandstones and mudstones. The ages of its interstratified volcanic rocks and its youngest detrital zircons can be used to constrain its depositional age (Dickinson and Gehrels, 2009). In the Guolong section, a tuff horizon (sample 13GL104, Fig. 2) from the bottom of the Duoni Formation records a zircon U-Pb age of 122.5 ± 1.3 Ma (n = 30 MSWD = 1.2) (Fig. 8, Appendix A), implying that the Duoni Formation deposition began prior to approximately 123 Ma. The termination of the Duoni Formation deposition in the Guolong section is constrained by the age of the conformably overlying Langshan Formation, which yields a maximum age of ~115 Ma. These ages are compatible with the youngest detrital zircon ages (YC1σ(2+), refer to Dickinson and Gehrels, 2009) of 107–114 Ma in this region (Table 1, Fig. 6). Therefore, the Duoni Formation age is well constrained between ~123 Ma and 115 Ma in the southern part of the Coqen Basin. This constrained time period is within the age range from the volcanic rocks dated by Volkmer et al. (2007), yielding weighted mean zircon ages of 129.7 ± 7.5 Ma, 122.3 ± 5.5 Ma and 112.9 ± 8.9 Ma.

However, the lack of tuff or direct contact relationships with other strata in the northern Coqen Basin indicates that the Duoni Formation age in the northern part of the basin can only be approximately constrained by the age of its youngest detrital zircons. The youngest

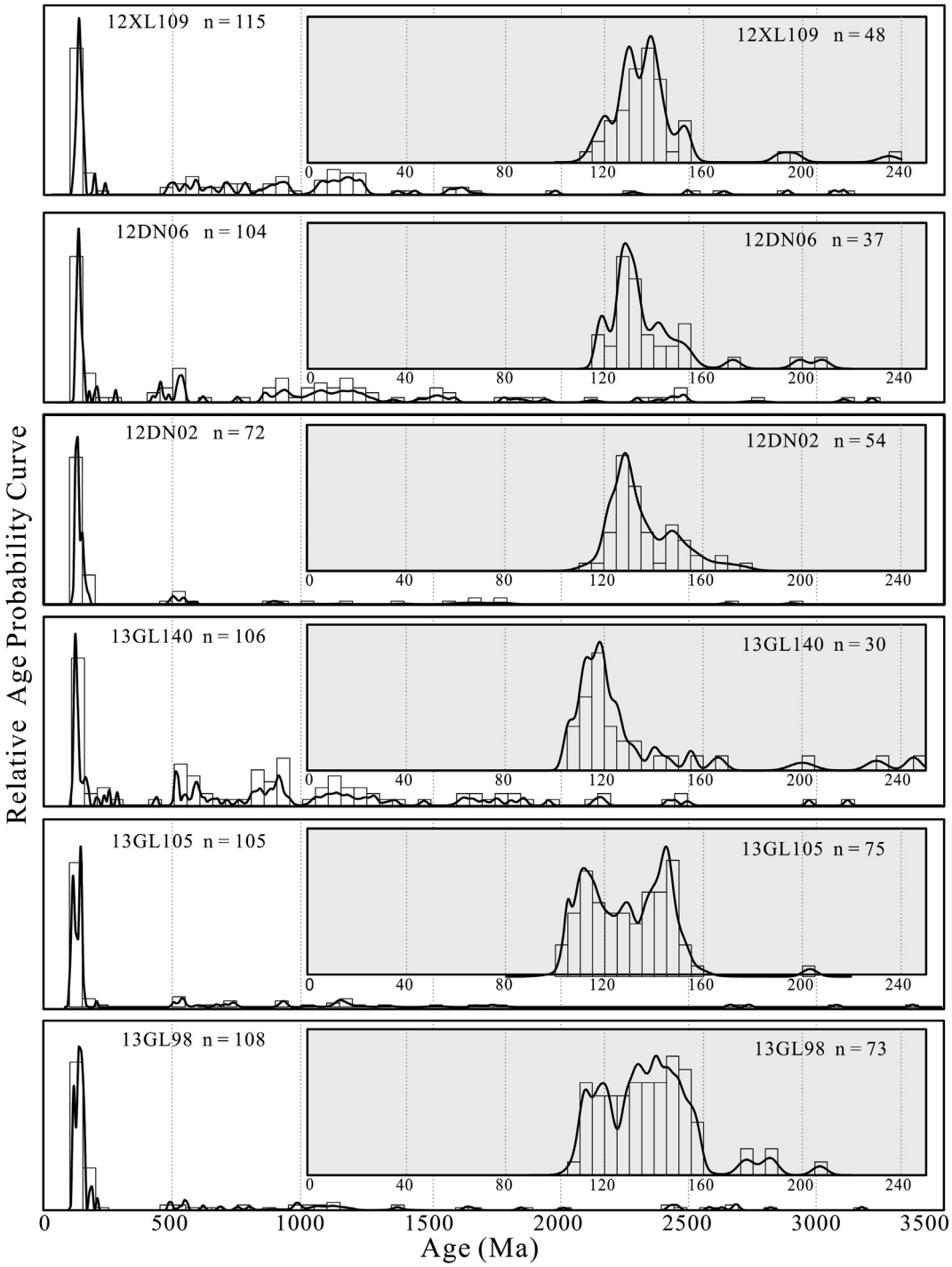

Fig. 6. Relative U-Pb age probabilities for detrital zircons from the sandstones of the Duoni Formation.

Please cite this article as: Sun, G., et al., Early Cretaceous palaeogeographic evolution of the Coqen Basin in the Lhasa Terrane, southern Tibetan Plateau, Palaeogeogr. Palaeoclimatol. Palaeoecol. (2017), http://dx.doi.org/10.1016/j.palaeo.2017.06.006

detrital zircons (YC1σ(2+)) in the north yield ages of 119–124 Ma (Table 1, Fig. 6), which implies that the Duoni Formation deposition in the north could have begun earlier than it did in the southern Coqen Basin.

6. Provenance analysis of the Duoni Formation

6.1. Provenance results

6.1.1. Sandstone modal compositions

A total of 22 analysed sandstones from the Guolong section are mostly moderately well sorted, contain siliceous or calcareous cements and feature a grain-supported texture. These sandstones have average modal compositions of Qt:F:L = 38:19:43 (see Appendix C, Fig. 7). Among these compositions, volcanic fragments and monocrystalline quartz are the main components of the samples and represent ~37% and ~34% of the total framework grains, respectively. Clasts of intermediate to felsic volcanic rocks dominate the volcanic fragments (Fig. 5A). In these sections, plagioclase is common but polycrystalline quartz is rare (Fig. 5B). The accessory minerals consist of zircon, rutile, tourmaline, muscovite and magnetite. On modal composition discrimination diagrams (Fig. 7, Dickinson et al., 1983; Garzanti et al., 2007), these samples mostly plot in the "magmatic arc" field and a few plot in the "recycled orogeny" region.

A total of 33 analysed sandstones from the Xialong and Zhukang sections record slightly different characteristics than those of the Guolong section. These samples contain siliceous cements and are supported by subrounded grains, which are medium- to well-sorted. They have average compositions of Qt:F:L = 75:9:16 (see Appendix C, Fig. 7). Monocrystalline quartz, which features clean surfaces and rounded shapes, comprises ~74% of the total framework grains (Fig. 5C and 7). Most of the rock fragments are dominated by sedimentary clasts and minor quantities of volcanic rocks. Analysis of some samples from the Zhukang section reveals that volcanic rocks are the main component of the rock fragments and can comprise up to ~30% of the total framework grains (see Appendix C). Collectively, these samples are distributed in the "recycled orogeny" and "magmatic arc" fields on the Qt-F-L and Qp-Lv-Ls diagrams (Fig. 7, Dickinson et al., 1983; Garzanti et al., 2007).

6.1.2. Detrital zircon U-Pb ages

A total of 608 detrital zircons were selected from 6 sandstones of the Duoni Formation for U-Pb dating by LA-ICPMS (Appendix A, Fig. 6). In detail, three samples, 13GL98, 13GL105 and 13GL140 were collected from the bottom, middle and upper parts of the Guolong section, respectively (refer to Fig. 2). Of the 108 dated zircons from sample 13GL98, 73 record age populations between 160 and 110 Ma, with peaks at ~120 and ~140 Ma. The other 35 zircons record pre-Mesozoic ages with peaks at ~550, ~950 and ~1200 Ma. A total of 105 detrital zircons from the sample 13GL105 record a major age population (75 of 105 zircons) between 160 and 103 Ma (with peaks at ~145 and 115 Ma), with additional age clusters (30 of 105 zircons) at ~550 and ~1150 Ma. A total of 106 zircons from the sample 13GL140 yield a large population between 125 and 105 Ma (peaking at ~120 Ma), and additional clusters at ~550, ~950, ~1200, ~1650 and ~2500 Ma.

U-Pb dating was also performed on 3 samples (12DN02, 12DN06 and 13XL09, Fig. 6) collected from the Xialong section. A total of 54 of 72 detrital zircons from the sample 12DN02 yield age populations between 160 and 119 Ma (peaking at ~150 and 130 Ma), with the youngest zircon ages falling at 113 ± 4 Ma, 119 ± 4 Ma and 120 ± 3 Ma. Among the 104 detrital zircon ages obtained from the sample 12DN06, 37 zircons record Mesozoic ages of 155–120 Ma, with a peak at ~130 Ma. The other 67 zircons yield age ranges of 550–500, 1200–900, and 1600–1500 Ma. The youngest ages in this sample are 118 ± 2 Ma, 118 ± 2 Ma and 119 ± 2 Ma. The sample 13XL109 yields a similar age distribution as 12DN06, with a main age population between 155 and 114 Ma (48 of 115 detrital zircons), and peaks at ~140 and 130 Ma. The pre-Mesozoic zircons (67 zircons) yield age ranges of 600–500, 1250–1050 and 1650–1550 Ma. The youngest ages in this sample are 114 ± 3 Ma, 116 ± 2 Ma and 119 ± 2 Ma.

6.1.3. Detrital zircon Hf isotopes

In total, 315 zircons from the above U-Pb dated detrital zircons were selected for in situ Hf isotopic analysis by MC-LA-ICPMS (Fig. 10, Appendix B). A total of 77 Mesozoic zircons from the Guolong section yield low $^{176}Hf/^{177}Hf$ initial ratios (0.282163–0.282620) and negative $\varepsilon_{Hf}(t)$ values of −18.7 to −2.7. Only 3 zircons from this section yield high $^{176}Hf/^{177}Hf$ initial ratios and positive $\varepsilon_{Hf}(t)$ values of +1.0 to +2.2. The other 55 pre-Mesozoic zircons yield a large range of $^{176}Hf/^{177}Hf$ initial ratios with $\varepsilon_{Hf}(t)$ values of −25.4 to +22.8. The Xialong section records similar trends as the Guolong section. A total of 99 Mesozoic zircons yield low $^{176}Hf/^{177}Hf$ initial ratios and negative $\varepsilon_{Hf}(t)$ values of c14.6 to −2.8. The other 85 pre-Mesozoic zircons yield scattered values of $^{176}Hf/^{177}Hf$ initial ratios and $\varepsilon_{Hf}(t)$ values (−30.8 to +22.9).

6.2. Provenance interpretation

Among the 608 dated detrital zircons of the Duoni Formation, 317 zircons (~52%) yield a significant age population ranging between 160 and 100 Ma, with a peak at ~130 Ma (Fig. 9). The Hf isotopic compositions of these zircons are characterized by their low $^{176}Hf/^{177}Hf$ initial ratios and negative $\varepsilon_{Hf}(t)$ values. These zircon characteristics are different from those of the northern Tibetan Plateau (such as the Songpan-Ganzi Terrane). which record an age population of 500–200 Ma (Weislogel et al., 2006; Gehrels et al., 2011; Ding et al., 2013), and are also different from those of the Qiangtang Terrane, which tend to record ages of 220–190 Ma (Leier et al., 2007b). The southern Lhasa subterrane

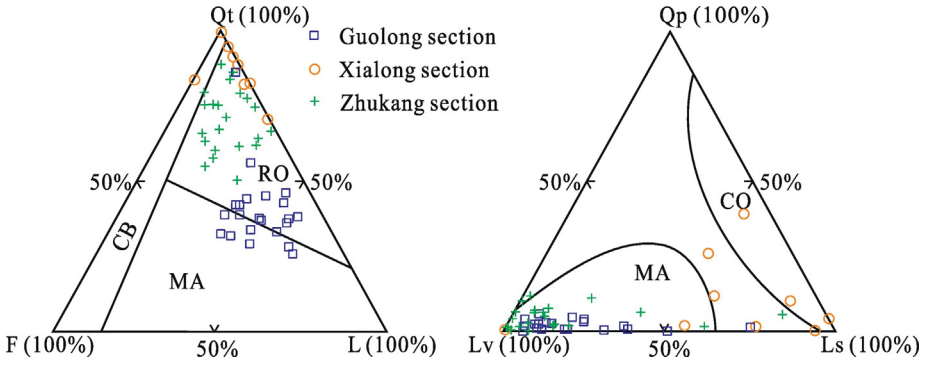

Fig. 7. The Ternary diagrams of sandstone framework compositions from the Duoni Formation. CB—continental terrane provenance; RO—recycled orogen provenance; MA—magmatic arc provenance (Dickinson et al., 1983; Garzanti et al., 2007); Qp—polycrystalline quartz; Qt—total quartz (monocrystalline quartz + Qp); L—total nonquartzose lithic grains; Lv—volcanic fragment; Ls—sedimentary rock fragment; F—total feldspar.

Please cite this article as: Sun, G., et al., Early Cretaceous palaeogeographic evolution of the Coqen Basin in the Lhasa Terrane, southern Tibetan Plateau, Palaeogeogr. Palaeoclimatol. Palaeoecol. (2017), http://dx.doi.org/10.1016/j.palaeo.2017.06.006

(i.e., the Gangdese magmatic arc and Xigaze forearc basin) has abundant Mesozoic zircons with ages ranging between 210 and 65 Ma. The Mesozoic zircons from the southern Lhasa subterrane record high $^{176}Hf/^{177}Hf$ initial ratios and positive $\varepsilon_{Hf}(t)$ values (Fig. 10, Chu et al., 2006; Ji et al., 2009a; Zhu et al., 2011a; Wu et al., 2010; An et al., 2014), which are inconsistent with the detrital zircons of the Duoni Formation. However, Mesozoic magmatism is also widespread in the northern Lhasa subterrane, especially in the Lower Cretaceous Zenong volcanic rocks within the Coqen Basin (Fig. 9, Zhu et al., 2008, 2011a). Igneous zircons in these Lower Cretaceous magmatic rocks record age populations ranging between 130 and 107 Ma, with low $^{176}Hf/^{177}Hf$ initial ratios and negative $\varepsilon_{Hf}(t)$ values (Chu et al., 2006; Zhu et al., 2008, 2009, 2011a) that are distinct from those of the Gandese magmatic arc to the south. Based on the contrasting natures of their zircons, it is likely that the clastic rocks of the Duoni Formation were derived from the volcanic rocks of the northern Lhasa subterrane. The Lower Cretaceous Zenong volcanic rocks in the Coqen Basin are the most likely sources for these Cretaceous zircons. The modal compositions of the sandstones from the Guolong section record abundant volcanic rock fragments and a "magmatic arc" source (Fig. 7), which are consistent with the above detrital zircon results. The palaeocurrent data of the Duoni Formation in the Guolong section also record a roughly northward direction, which further confirms the above interpretation.

In addition, the pre-Mesozoic zircons (~48% of total zircons) yield age ranges of 600–500 Ma, 1000–900 Ma, 1250–1050 Ma, 2100–1700 Ma and ~2500 Ma. The ages of these pre-Mesozoic zircons are consistent with the current published detrital zircon ages from the Paleozoic sedimentary strata in the Lhasa Terrane, which are characterized by age populations of 600–500 Ma, 1300–1050 Ma, 1950–1700 Ma and ~2500 Ma (Gehrels et al., 2011; Leier et al., 2007c; Zhu et al., 2011b). Meanwhile, many sandstones from the Xialong section contain abundant quartz clasts and sedimentary rock fragments and are distributed within the "recycled orogen" field on Qt-F-L and Qp-Lv-Ls diagrams (Fig. 7). In conclusion, the Lower Cretaceous Zenong volcanic rocks in the northern Lhasa subterrane contain zircons from the underlying Paleozoic sedimentary bedrocks, which then also generated old zircons.

The results of previously published studies of the Lower Cretaceous clastic rocks in the northern regions of the Lhasa basins indicate that they had two significant sedimentary sources: the Gangdese magmatic arc to the south (Zhang et al., 2011), and the Bangong-Nujiang suture and Qiangtang Terrane to the north (Leeder et al., 1988; Murphy et al., 1997; Leier et al., 2007a). In this study, we demonstrate that the U-Pb ages and Hf isotopic compositions of detrital zircons from the Early Cretaceous Coqen Basin indicate that they were derived from Lower Cretaceous Zenong volcanic rocks and the underlying sedimentary bedrock (comprising Paleozoic strata) exposed on the northern Lhasa subterrane. This finding is comparable to results from other basins within the northern Lhasa subterrane.

7. Palaeogeographic reconstruction and regional implications

7.1. Stratigraphic framework and depositional model for the Coqen Basin

In the Coqen Basin, the Zenong volcanic rocks are exposed in the southern region of the Guolong section (Fig. 1B). The published zircon ages of the Zenong volcanic rocks in the Coqen Basin indicate that they were erupted between ~130–107 Ma (Zhu et al., 2008, 2009, 2011a and references therein), thus, implying that they are time-equivalent to the Duoni and Langshan Formations, which range in age from ~123 to 98 Ma, although the Duoni Formation conformably overlies the Zenong volcanic rocks in the Guolong section (Fig. 2). The large benthic foraminifera of the Langshan limestone and the zircon U-Pb ages of the Duoni Formation yield additional chronostratigraphic constraints for the Coqen Basin. These ages demonstrate that Lower Cretaceous clastic rocks began accumulating at ~123 Ma; this was followed by a diachronous phenomenon in the Coqen Basin in which the Langshan Formation began to develop in the northern region of the basin ca. 119 Ma, whereas the Duoni Formation continued to accumulate in the southern region until ~115 Ma. Collectively, in the Coqen Basin, it is hypothesized that the eruption of the Zenong volcanic rocks occurred

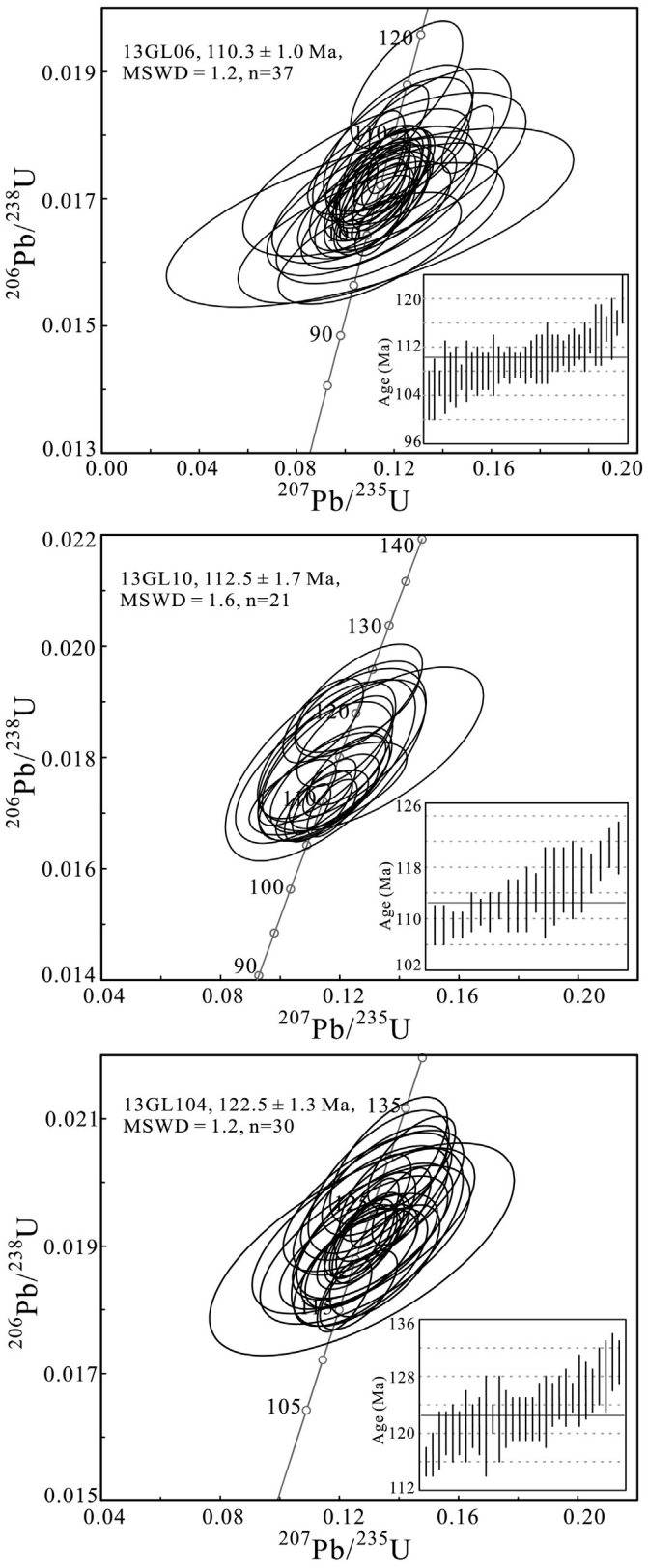

Fig. 8. The U-Pb zircon weighted mean ages and concordia diagrams of the tuff horizon in the Duoni and Langshan Formations from the Guolong section.

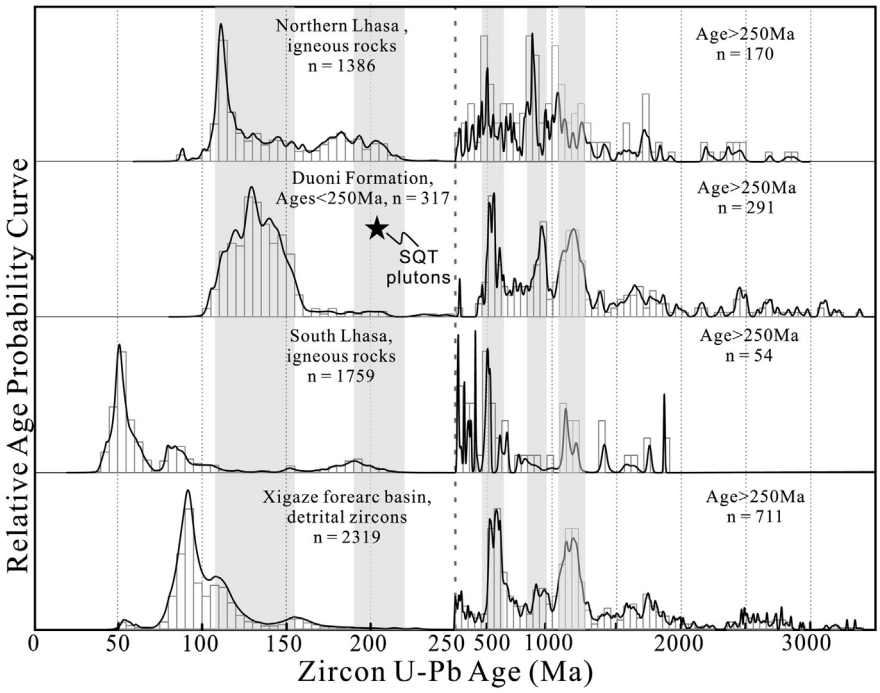

Fig. 9. Comparisons of probability density diagrams of detrital zircon ages from the Duoni Formation (this study) to reference populations from the southern Lhasa subterrane (Zhang et al., 2007a; Lee et al., 2007, 2009; Wen et al., 2008; Chu et al., 2006, 2011; Ji et al., 2009; Zhu et al., 2009, 2011a), northern Lhasa subterrane (Murphy et al., 1997; Chu et al., 2006; Guynn et al., 2006; Zhang et al., 2007b; He et al., 2006a, 2006b; Kapp et al., 2003, 2005; Liu et al., 2006; Volkmer et al., 2007; Zhou et al., 2008; Meng et al., 2010; Zhu et al., 2009, 2011a), and Xigaze forearc basin (Wu et al., 2010; An et al., 2014; Orme et al., 2014). Note the change of scale at 250 Ma. SQT plutons—southern Qiangtang terrane plutons.

during the deposition of both the Duoni and Langshan Formations, thus, indicating that these three formations were diachronous during the Early Cretaceous.

As described above, the depositional environment of the Duoni Formation in the Coqen Basin records a more distal trend towards the north (from the Guolong section in the south to the Xialong and Zhukang sections in the north), moving from a fluvial environment to a more shelf-coastal environment. This provenance analysis reveals that the Duoni Formation in the Guolong section was primarily derived from the Zenong volcanic rocks to the south, whereas the Zhukang and Xialong sections also contain recycled components of the Palaeozoic sedimentary bedrocks of the northern Lhasa subterrane in addition to the Zenong volcanic rocks. The northward fluvial pattern and the south-to-north deepening trend of the depositional system imply that the depocentre of the Coqen Basin was located in the north during this time interval. The Langshan Formation, which conformably overlies the Duoni Formation, is widespread across the Coqen Basin and records deposition within a low-energy shallow-marine environment during the Early Cretaceous. The Langshan Formation thins from north to south (i.e., it is only ~80 m thick in the southernmost region of the basin; refer to section SE01 in Sun et al., 2015), which further implies that the depocentre occurred in the northern region of the basin (Fig. 11).

Therefore, based on the sedimentology, geochronology and provenance analyses of the Duoni and Langshan Formations performed in this study, the depositional model of the Coqen Basin is composed of two stages described below.

The first stage (~123–115 Ma, Fig. 12A): The Duoni Formation was well developed in the Coqen Basin, featuring a fluvial environment in the southern region of the basin and a shelf-coastal environment in the north; thus, this implies that the depocentre occurred in the northern region of the basin. Concurrently, the eruption of the Zenong volcanic rocks occurred near the southern part of the Coqen Basin, causing

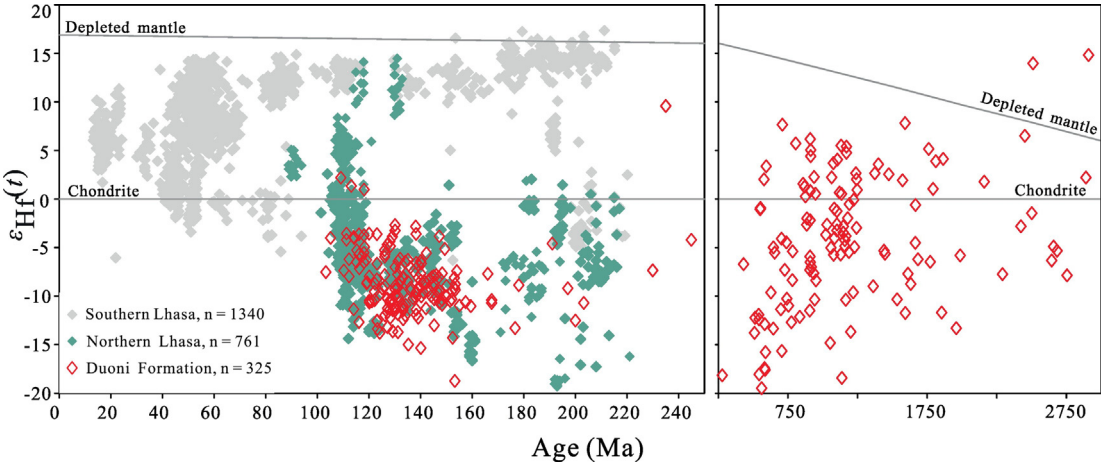

Fig. 10. Plots of εHf(t) values versus the U-Pb ages of detrital zircons from sandstones within the Duoni Formation. Data of the southern Lhasa subterrane are from Chu et al. (2006), Zhang et al. (2007a), Lee et al. (2007), Ji et al. (2009), and Zhu et al. (2009, 2011a); those of the northern Lhasa subterrane are from Chu et al. (2006), Zhang et al. (2007b), and Zhu et al. (2011a).

Please cite this article as: Sun, G., et al., Early Cretaceous palaeogeographic evolution of the Coqen Basin in the Lhasa Terrane, southern Tibetan Plateau, Palaeogeogr. Palaeoclimatol. Palaeoecol. (2017), http://dx.doi.org/10.1016/j.palaeo.2017.06.006

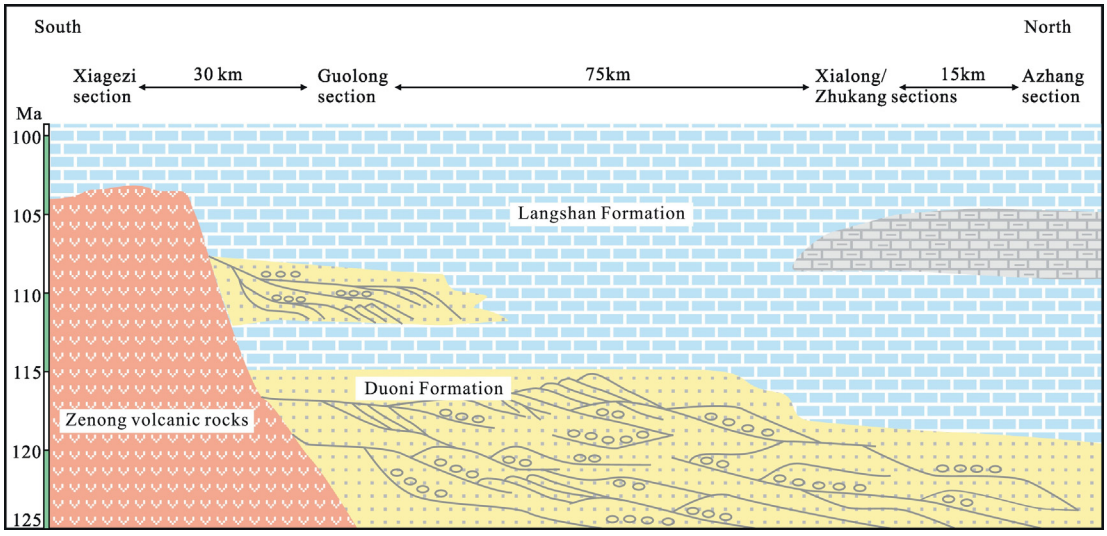

Fig. 11. Sketched map for the basin architecture of the Early Cretaceous Coqen Basin, Xiagezi section can be referred to the section SE01 in Sun et al. (2015).

the Duoni Formation in the Guolong section to be primarily sourced from these volcanic rocks. In addition, most of the Palaeozoic sedimentary strata were recycled into the northern sections of the Duoni Formation. At ~119 Ma, the sea transgressed southward and shallow-marine limestones accumulated in the Azhang section in the northern Coqen Basin.

The second stage (~115–98 Ma, Fig. 12B): During this time interval, southward transgression resulted in the entire basin being submerged, creating a shallow-marine environment for the accumulation of the rudist- and *Orbitolina*-bearing limestones of the Langshan Formation. Due to relative sea level changes in the southern region of the basin, the Langshan Formation records the progradation of fluvial systems into the basin from ~113–110 Ma. From 107 to 102 Ma, low-energy lagoonal conditions developed in the northern region of the basin.

7.2. Broader Early Cretaceous palaeogeography of the Lhasa Terrane

Many sedimentary basins developed from the north to the south of the Lhasa Terrane during the Cretaceous and accumulated thick marine-terrestrial successions (such as the southern Nima Basin, the Selin Co Basin, and the Linzhou Basin). Previous studies have recorded the sedimentology and provenance of these basins (Zhang et al., 2004, 2011; Leier et al., 2007a; Kapp et al., 2007a; Orme et al., 2014, Orme and Laskowaki, 2016; An et al., 2014). The Early Cretaceous basins are comparable in the Lhasa Terrane (Fig. 13). Here, we synthesise the stratigraphic data from these Early Cretaceous basins in the Lhasa Terrane to reconstruct their palaeogeography.

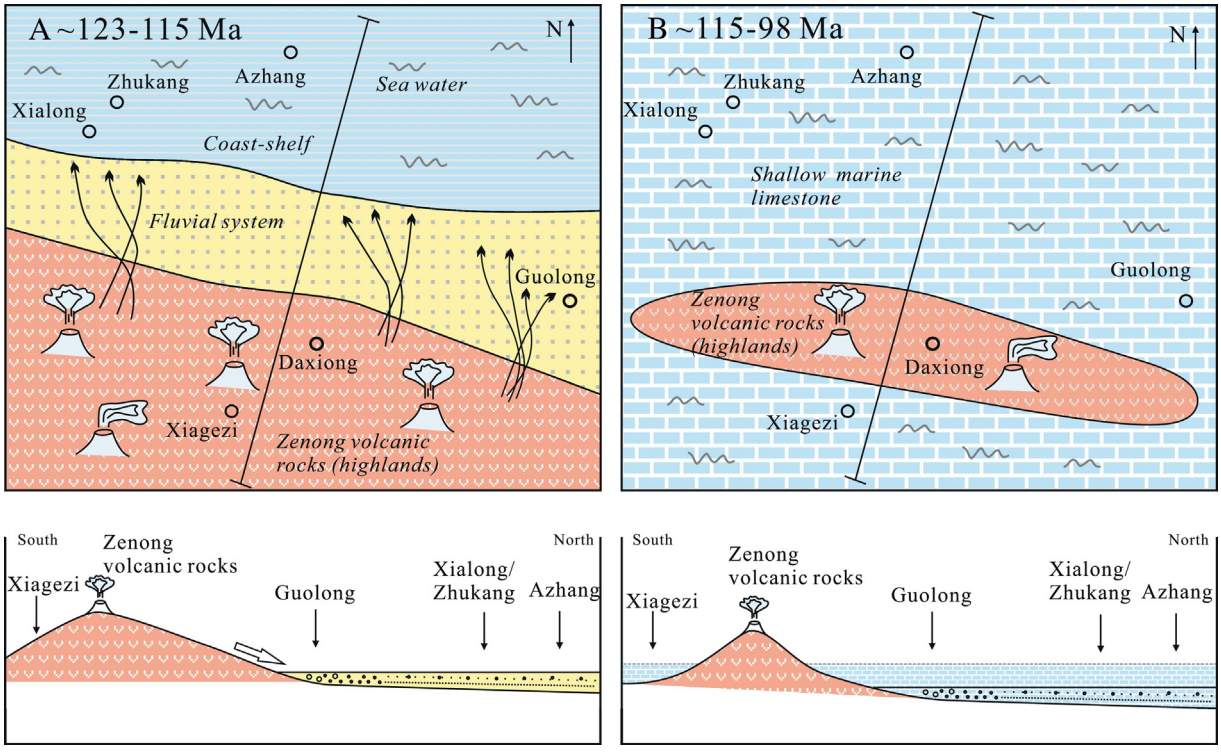

Fig. 12. Sketched maps for the different depositional stages of the Early Cretaceous Coqen Basin.

During the earliest period of the Cretaceous (>123 Ma), extensive volcanism developed in the northern Lhasa subterrane, which is composed of the Zenong volcanic rocks and their time-equivalent intrusive rocks (e.g., Xu et al., 1985; Harris et al., 1990; Chu et al., 2006; Zhu et al., 2009, 2011a). During this time, there is no deposition recorded in the Coqen Basin; alternatively, the accumulation of widespread Zenong volcanic rocks is recorded. In the Nima Basin on the northern margin of the Lhasa Terrane, Late Jurassic-Early Cretaceous marine sandstones preceded Early Cretaceous continental deposits. There is an angular unconformity between the marine and terrestrial strata with an age range of ~125–118 Ma, which is interpreted to reflect the collision of the Lhasa-Qiangtang Terranes along the Bangong-Nujiang suture zone (Kapp et al., 2007a). The Selin Co and Linzhou Basins further document the presence of deep-water turbidites and shallow-marine clastic deposition at this time (Zhang et al., 2011; Leier et al., 2007a).

From ~123–115 Ma (Fig. 14A), magmatism continued to occur in the northern Lhasa subterrane. In addition, the Duoni Formation, which is composed of shallow-marine deposits and fluvial systems, was widespread throughout the majority of the northern Lhasa subterrane. These medium- to coarse-grained sandstones and conglomerates were primarily sourced from the time-equivalent Lower Cretaceous Zenong volcanic rocks. Similar sedimentological and provenance characteristics are also observed in other basins (i.e., the Selin Co and Linzhou Basins, Leier et al., 2007a; Xie et al., 2007; He et al., 2007; Zhang et al., 2011). However, the Nima Basin contains continental deposits above the angular unconformity (Kapp et al., 2007a; DeCelles et al., 2007). During this time interval, the Xigaze forearc basin was initiated on the southern Lhasa subterrane with the deposition of deep-water radiolarian cherts and several fine-grained sandstones in a deep sea plain environment (An et al., 2014; Wang et al., 2017), which imply that the southern Gangdese magmatic arc could not have been exhumed at this time.

From ~115–98 Ma, the northernmost Lhasa subterrane was a predominantly marine environment, in which the thick Langshan foraminifera- and rudist-rich limestones were deposited (i.e., the Coqen Basin, Selin Co Basin, and Linzhou Basin, Fig. 14B, Zhang et al., 2004, 2011; Leier et al., 2007a). The Langshan Formation tends to thin from the north to south, thus, implying that the depocentre was located in the north. In some places, clastic rocks accumulated due to changes in sea level. Concurrently, terrestrial deposits continued to develop in the Nima Basin, whereas in the south, the Xigaze forearc basin contains thick deep-water turbidites and fan-deltaic deposits sourced from the widespread Gangdese magmatic arc (Wu et al., 2010; An et al., 2014; Orme et al., 2014; Orme and Laskowaki, 2016).

7.3. The controls of basin evolution for northern Lhasa

The early tectonic evolution of the Tibetan Plateau, and particularly the tectonic framework of the southern Asia margin prior to the India-Asia collision, remains controversial (Murphy et al., 1997; Zhang, 2000; Zhang et al., 2004; Kapp et al., 2007b). Sedimentological analysis in the Coqen Basin indicates that continental fluvial environments developed during the Duoni Formation deposition. Similarly, fluvial environments were also developed in the Linzhou Basin to the east (Leier et al., 2007a). Concurrently, marginal marine to deep-water

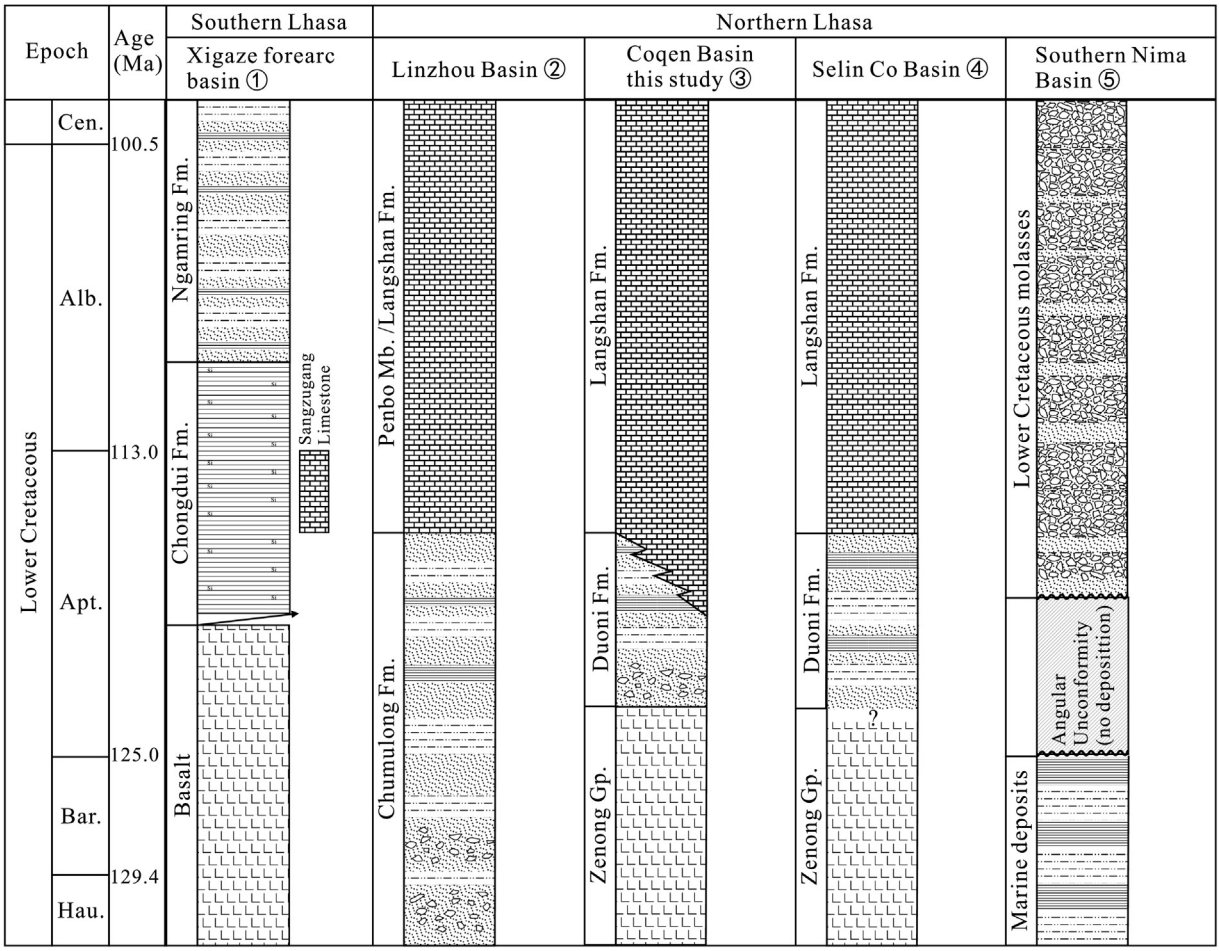

Fig. 13. Comparisons of the Lower Cretaceous strata in the Xigaze forearc basin, Linzhou basin, southern Nima Basin, Selin Co Basin, and Coqen Basin (this study). The strata and time scale in ordinate are referred to in An et al. (2014), Xie et al. (2007), Kapp et al. (2007a), DeCelles et al. (2007), Leier et al. (2007a) and Zhang et al. (2011). See Fig. 4 for the lithological legend, and Fig. 14 for the basin locations. Hau.—Hauterivian; Bar.—Barrenmian; Apt.—Aptian; Alb.—Albian; Cen.—Cenomanian; Mb. —Member; Fm. —Formation; Gp. —Group.

Please cite this article as: Sun, G., et al., Early Cretaceous palaeogeographic evolution of the Coqen Basin in the Lhasa Terrane, southern Tibetan Plateau, Palaeogeogr. Palaeoclimatol. Palaeoecol. (2017), http://dx.doi.org/10.1016/j.palaeo.2017.06.006

environments developed along the northern margin of the northern Lhasa subterrane (Zhang et al., 2004, 2011); thus, this implies that the depositional environment water depth tended to be deeper from south to north and the depocentre was located in the north. This is consistent with the provenance results that indicated the Lower Cretaceous Duoni Formation was primarily sourced from the Lower Cretaceous Zenong volcanic rocks to the south. The palaeocurrent data also implies that northward-flowing fluvial patterns are present in the Coqen Basin study area (Fig. 12). The south-north basin deepening could be produced by foreland flexure loading in response to the Lhasa-Qiangtang collision along the Bangong-Nujiang suture zone, which is confirmed by a ~ 125–118 Ma unconformity in the Nima Basin (Kapp et al., 2007a) and a peripheral foreland basin model established in the Selin Co-Linzhou area (Kapp et al., 2007a; Leier et al., 2007a). However, this model fails to interpret the provenance results in the Coqen Basin. As previously discussed, the Zenong volcanic rocks erupted continuously during the Early Cretaceous, thus, being concurrent with the Duoni Formation deposition. In combination with the provenance results, the Duoni Formation deposition could be primarily controlled by the enhanced magmatic activities in the northern Lhasa subterrane during the Early Cretaceous. This is supported by the abundant tuff interbedded horizons and the volcanic fragments in the Duoni Formation (Volkmer et al., 2007). This magmatic activity-influenced basin framework in the hinterland is similar to the Miocene-Pliocene volcanic controls of sedimentation in the Famatina Ranges, southern Central Andes (Martina et al., 2006). In some areas of the northern Lhasa subterrane, the abundance of recycled sedimentary detritus in the sandstones of the study area reveals that the magmatic rocks were eroded and cut into the underlying Palaeozoic bedrocks.

Since ~119 Ma, sea water began intruding from the northern margin of the Lhasa Terrane and gradually moved southward (~115 Ma). Subsequently, the majority of the northern Lhasa subterrane, except for the volcanic-influenced highlands, was covered by sea water and the shallow-marine Langshan limestone accumulated until ~98 Ma (Fig. 14B, Zhang et al., 2011; Leier et al., 2007a). The limestone age trend indicates that the north is slightly older than the south, which is consistent with this southward transgression. At this time, the depocentre should remain in the north, which is confirmed by the south-to-north limestone thickening (Fig. 11). However, this transgression mechanism is subtle for interpretation. A eustatic sea level rise is an easy interpretation for this widespread shallow-marine Langshan limestone in the northern Lhasa subterrane. Additionally, considering the northern Lhasa tectonic setting, both the Lhasa-Qiangtang collision to the north and the Neo-tethyan oceanic lithosphere beneath the Lhasa Terrane to the south (Yin and Harrison, 2000; Zhu et al., 2013) can result in accommodation space due to foreland flexure deformation and dynamic

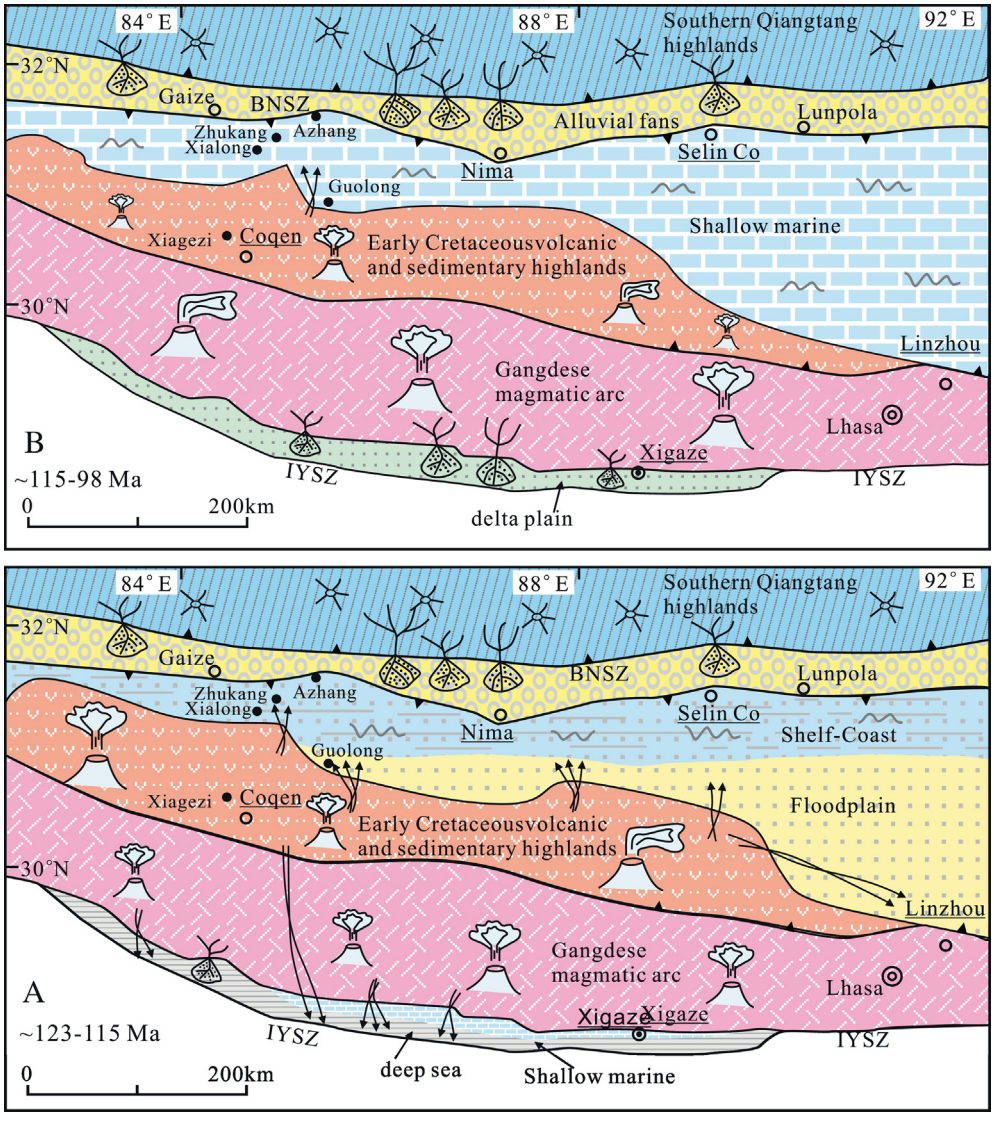

Fig. 14. The reconstruction of the paleogeography of the Early Cretaceous Lhasa Terrane. BNSZ—Bangong-Nujiang suture zone; IYSZ—Indus-Yarlung suture zone.

Please cite this article as: Sun, G., et al., Early Cretaceous palaeogeographic evolution of the Coqen Basin in the Lhasa Terrane, southern Tibetan Plateau, Palaeogeogr. Palaeoclimatol. Palaeoecol. (2017), http://dx.doi.org/10.1016/j.palaeo.2017.06.006

subsidence, respectively. A single mechanism or a combination of mechanisms used to interpret this transgression requires additional data in future studies before thoroughly understanding the tectonic history of the south Asia margin prior to India-Asia collision.

8. Conclusions

The results of the sedimentologic, stratigraphic and geochronologic analyses of the Early Cretaceous Coqen Basin, when combined with the results of other basin studies in the Lhasa Terrane, yield several conclusions that are described below.

1) The Early Cretaceous Coqen Basin includes the Duoni and Langshan Formations. The Duoni Formation was deposited in a fluvial environment to the south and a shelf-coastal environment to the north. The Langshan Formation is primarily composed of *Orbitolina*-rich limestones. Geochronologic and micropalaeontological analyses indicate that the Duoni and Langshan Formations were deposited from ~ 123–98 Ma.
2) The Duoni Formation provenance analysis implies that this formation was primarily sourced from the Lower Cretaceous Zenong volcanic rocks and Palaeozoic sedimentary bedrock from the northern Lhasa subterrane. This interpreted provenance is different compared to previous studies and implies that the northern Lhasa subterrane is the source area for the inner basins during the Early Cretaceous.
3) The palaeogeographic reconstruction of the Lhasa Terrane indicates that the basin evolution can be divided into two stages. In the first stage (~123–115 Ma), basins on the northern Lhasa subterrane were dominated by the fluvial-marginal Duoni Formation, that was controlled by coeval magmatic activities; in the second stage (~115–98 Ma), most of the northern Lhasa subterrane was covered by the shallow-marine Langshan limestone, influenced by a north-south transgression.

Supplementary data to this article can be found online at http://dx.doi.org/10.1016/j.palaeo.2017.06.006.

Acknowledgments

We appreciate that Bin Wu, Zhiyong Zhu, Xiong Yan, Juan Li, and Xuan Lv provided much help in analyzing the zircon U-Pb ages and Hf isotopes. We thank Zhong Han and Wei Zhang for their assistance in the field. This study was financially supported by the National Natural Science Foundation of China Project (41472081, 41602104), Natural Science Foundation of Jiangsu province (BK20160858), the Fundamental Research Funds for the Central Universities of China (2015B11414) and the Open Research Funds from the State Key Laboratory for Mineral Deposits Research, Nanjing University (2017-LAMD-K09). We are grateful to Thomas Algeo for his comments and editorial handling, and Peter Cawood and Paul Kapp for their critical and constructive comments that improved this paper.

References

Allen, J.R.L., 1964. Studies in fluvial sedimentation: six cyclothems from the lower Old Red Sandstone, Anglo Welsh basin. Sedimentology 3, 163–198.
An, W., Hu, X., Garzanti, E., Marcelle, M.K., Wang, J., Sun, G., 2014. Xigaze Forearc Basin (South Tibet) revisited: unroofing of the Gangdese arc and origin of the Xigaze ophiolite. Geol. Soc. Am. Bull. 126, 1595–1613.
Andersen, T., 2002. Correction of common lead in U-Pb analyses that do not report ^{204}Pb. Chem. Geol. 192, 59–79.
BouDagher-Fadel, M.K., Hu, X.M., Price, G.D., Sun, G.Y., Wang, J.G., An, W., 2017. Foraminiferal biostratigraphy and paleoenvironmental analysis of the mid-Cretaceous limestones in the southern Tibetan Plateau. J. Foraminifer. Res. 47, 188–207.
Bouvier, A., Vervoort, J.D., Patchett, P.J., 2008. The Lu-Hf and Sm-Nd isotopic composition of CHUR: constraints from unequilibrated chondrites and implications for the bulk composition of terrestrial planets. Earth Planet. Sci. Lett. 273, 48–57.
Bridge, J.S., 2009. Rivers and Floodplains: Forms, Processes, and Sedimentary Record. Blackwells, Oxford (pp. 487).
Burg, J.P., Proust, F., Tapponnier, P., Chen, G.M., 1983. Deformation phases and tectonic evolution of the Lhasa block, China. Eclogae Geol. Helv. 76, 643–665.
Cant, D.J., Walker, R.G., 1978. Fluvial processes and facies sequences in the sandy braided South Saskatchewan River, Canada. Sedimentology 25, 625–648.
Cawood, P.A., Hawkesworth, C.J., Dhuime, B., 2012. Detrital zircon record and tectonic setting. Geology 40, 875–878.
Chu, M., Chung, S., Song, B., Liu, D., O'Reilly, S., Pearson, N., Ji, J., Wen, D., 2006. Zircon U-Pb and Hf Isotope Constraints on the Mesozoic tectonics and crustal evolution of Southern Tibet. Geology 34, 745–748.
Chu, M., Chung, S., O'Reilly, S., Pearson, N., Wu, F., Li, X., Liu, D., Ji, J., Chu, C., Lee, H., 2011. India's hidden inputs to Tibetan orogeny revealed by Hf isotopes of Transhimalayan zircons and host rocks. Earth Planet. Sci. Lett. 307, 479–486.
DeCelles, P.G., Langford, R.P., Schwartz, R.K., 1983. Two new methods of paleocurrent determination from trough cross-stratifi cation. J. Sediment. Petrol. 53, 629–642.
DeCelles, P.G., Kapp, P., Ding, L., Gehrels, G.E., 2007. Late Cretaceous to mid-Tertiary basin evolution in the central Tibetan Plateau: changing environments in response to tectonic partitioning, aridification, and regional elevation gain. Geol. Soc. Am. Bull. 119, 654–680.
DeCelles, P.G., Kapp, P., Gehrels, G.E., Ding, L., 2014. Paleocene-Eocene foreland basin evolution in the Himalaya of southern Tibet and Nepal: implications for the age of initial India-Asia collision. Tectonics 33, 824–849.
Dewey, J.F., Shackleton, R.M., Chang, C., Yiyin, S., 1988. The tectonic evolution of the Tibetan Plateau. Philos. Trans. R. Soc. Lond. Ser. A 327, 379–413.
Dickinson, W., Gehrels, G., 2009. Use of U-Pb ages of detrital zircons to infer maximum depositional ages of strata: a test against a Colorado Plateau Mesozoic database. Earth Planet. Sci. Lett. 288, 115–125.
Dickinson, W.R., Beard, S.L., Brakenridge, G.R., Erjavec, J.L., Ferguson, R.C., Inman, K.F., Knepp, R.A., Lindberg, F.A., Ryberg, P.T., 1983. Provenance of North American Phanerozoic sandstones in relation to tectonic setting. Geological Society of America Bulletin 94, 222–235.
Diemer, J.A., Belt, E.S., 1991. Sedimentology and paleohydraulics of the meandering river systems of the Fort Union Formation, southeastern Montana. Sediment. Geol. 75, 85–108.
Ding, L., Kapp, P., Zhong, D., Deng, W., 2003. Cenozoic volcanism in Tibet: evidence for a transition from Oceanic to continental subduction. J. Petrol. 44, 1833–1865.
Ding, L., Yang, D., Cai, F.L., Pullen, A., Kapp, P., Gehrels, G.E., Zhang, L.Y., Zhang, Q.H., Lai, Q.Z., Yue, Y.H., Shi, R.D., 2013. Provenance analysis of the Mesozoic Hoh-Xil-Songpan-Ganzi turbidites in northern Tibet: implications for the tectonic evolution of the eastern Paleo-Tethys Ocean. Tectonics 32, 1–15.
Dürr, S.B., 1996. Provenance of Xigaze forearc clastic rocks (Cretaceous, south Tibet). Geol. Soc. Am. Bull. 108, 669–691.
England, P., Searle, M., 1986. The Cretaceous-Tertiary deformation of the Lhasa block and its implications for crustal thickening in Tibet. Tectonics 5, 1–14.
Festa, A., Pini, G.A., Dilek, Y., Codegone, G., 2010. Mélanges and mélange-forming processes: a historical overview and new concepts. Int. Geol. Rev. 52, 1040–1105.
Flügel, E., 2004. Microfacies of Carbonate Rocks: Analysis, Interpretation and Application. Springer-Verlag, Berlin, Germany, pp. 369–574p.
Garzanti, E., Doglioni, C., Vezzoli, G., Ando, S., 2007. Orogenic belts and orogenic sediment provenance. J. Geol. 115, 315–334.
Gehrels, G., Kapp, P., DeCelles, P., Pullen, A., Blakey, R., Weislogel, A., Ding, L., Guynn, J., Martin, A., Mcquarrie, N., Yin, A., 2011. Detrital zircon geochronology of pre-Tertiary strata in the Tibetan-Himalayan orogen. Tectonics 30, TC5016. http://dx.doi.org/10.1029/2011TC002868.
Griffin, W.L., Wang, X., Jackson, S.E., Pearson, N.J., O'Reilly, S.Y., 2002. Zircon geochemistry and magma mixing, SE China: in-situ analysis of Hf isotopes, Tonglu and Pingtan igneous complexes. Lithos 61, 237–269.
Guynn, J.H., Kapp, P., Pullen, A., Heizler, M., Gerhels, G.E., Lin, D., 2006. Tibetan basement rocks near Amdo reveal "missing" Mesozoic tectonism along the Bangong suture, central Tibet. Geology 34, 505–508.
Harris, N.B.W., Inger, S., Xu, R., 1990. Cretaceous plutonism in Central Tibet: an example of post-collision magmatism? J. Volcanol. Geotherm. Res. 44, 21–32.
He, Z.H., Yang, D.M., Wang, T.W., 2006a. The determination of Early Cretaceous post-collision granitoids in Sangba area of Gangdese tectonic belt and its tectonic significance. Acta Petrol. Mineral. 25, 185–193.
He, Z.H., Yang, D.M., Zheng, C.Q., Wang, T.W., 2006b. Isotopic dating of the Mamba granitoid in the Gangdise Tectonic Belt and Its Constraint on the Subduction Time of the Neotethys. Geological Review 52, 100–106 (in Chinese with English abstract).
He, S., Kapp, P., DeCelles, P.G., Gehrels, G.E., Heizler, M., 2007. Cretaceous-Tertiary geology of the Gangdese Arc in the Linzhou area, southern Tibet. Tectonophysics 433, 15–37.
Hu, X.M., Garzanti, E., Moore, T., Raffi, I., 2015. Direct stratigraphic dating of India-Asia collision onset at the Selandian (middle Paleocene, 59 ± 1 Ma). Geology 43, 859–862.
Hu, X.M., Garzanti, E., Wang, J.G., Huang, W.T., An, W., Webb, A., 2016. The timing of India-Asia collision onset–facts, theories, controversies. Earth Sci. Rev. 160, 264–299.
Hu, X.M., Wang, J.G., An, W., Garzanti, E., Li, J., 2017. Constraining the timing of the India-Asia continental collision by the sedimentary record. Sci. China Earth Sci.:1–23 http://dx.doi.org/10.1007/s11430-016-9003-6.
Ingersoll, R.V., Bullard, T.F., Ford, R.L., Grimm, J.P., Pickle, J.D., Sares, S.W., 1984. The effect of grain size on detrital modes: a test of the Gazi-Dickinson pointcounting method. J. Sediment. Petrol. 54, 103–116.
Jackson, S.E., Pearson, N.J., Griffin, W.L., Belousova, E.A., 2004. The application of laser ablation-inductively coupled plasma-mass spectrometry to in situ U/Pb zircon geochronology. Chem. Geol. 211, 47–69.
Ji, W.Q., Wu, F.Y., Chung, S.L., Li, J.X., Liu, C.Z., 2009. Zircon U-Pb geochronology and Hf isotopic constraints on petrogenesis of the Gangdese Batholith, Southern Tibet. Chem. Geol. 262, 229–245.

Please cite this article as: Sun, G., et al., Early Cretaceous palaeogeographic evolution of the Coqen Basin in the Lhasa Terrane, southern Tibetan Plateau, Palaeogeogr. Palaeoclimatol. Palaeoecol. (2017), http://dx.doi.org/10.1016/j.palaeo.2017.06.006

Johnson, H.D., Baldwin, C.T., 1996. Shallow clastic seas. In: Reading, H.G. (Ed.), Sedimentary Environments: Processes, Facies and Stratigraphy, Third Edition. Blackwell Science, Oxford, U.K., pp. 232–280.

Kapp, P., Murphy, M.A., Yin, A., Harrison, T.M., Ding, L., Guo, J., 2003. Mesozoic and Cenozoic tectonic evolution of the Shiquanhe area of western Tibet. Tectonics 22 pp. 1029. http://dx.doi.org/10.1029/2001TC001332.

Kapp, P., Yin, A., Harrison, T.M., Ding, L., 2005. Cretaceous-Tertiary shortening, basin development, and volcanism in central Tibet. Geol. Soc. Am. Bull. 117, 865–878.

Kapp, P., Decelles, P.G., Gehrels, G.E., Heizler, M., Ding, L., 2007a. Geological records of the Lhasa-Qiangtang and Indo-Asian collisions in the Nima area of Central Tibet. Geol. Soc. Am. Bull. 119, 917–932.

Kapp, P., DeCelles, P.G., Leier, A.L., Fabijanic, J.M., He, S., Pullen, A., Gehrels, G.E., 2007b. The Gangdese retroarc thrust belt revealed. GSA Today 17 (pp, 7). http://dx.doi.org/10.1130/GSAT01707A.1.

Kirschbaum, M.A., 1989. Lagoonal deposits in the Upper Cretaceous Rock Springs Formation (Mesaverde Group), southwest Wyoming. In: Ward, L.G., Ashley, G.M. (Eds.), Physical Processes and Sedimentology of Siliciclastic-Dominated Lagoonal Systems. Marine Geology Vol. 88, pp. 349–364.

Kraus, M.J., 1999. Paleosols in clastic sedimentary rocks: their geologic applications. Earth Sci. Rev. 47, 41–70.

Kreisa, R.D., 1981. Storm-generated sedimentary structures in subtidal marine facies with examples from the Middle and Upper Ordovician of Southwestern Virginia. J. Sediment. Res. 51, 823–848.

Lee, H.Y., Chung, S.L., Wang, Y.B., Zhu, D.C., Yang, J.H., Song, B., Liu, D.Y., Wu, F.Y., 2007. Age, petrogenesis and geological significance of the Linzizong volcanic successions in the Linzhou Basin, Southern Tibet: evidence from zircon U-Pb dates and Hf isotopes. Acta Petrol. Sin. 23, 493–500.

Lee, H.Y., Chung, S.L., Lo, C.H., Ji, J.Q., Lee, T.Y., Qian, Q., Zhang, Q., 2009. Eocene Neotethyan slab breakoff in southern Tibet inferred from the Linzizong volcanic record. Tectonophysics 477, 20–35.

Leeder, M.R., Smith, A.B., Jixiang, Y., 1988. Sedimentology and paleoenvironmental evolution of the 1985 Lhasa to Golmud Geotraverse. Philos. Trans. R. Soc. Lond. Ser. A 327, 107–143.

Leier, A.L., Decelles, P.G., Kapp, P., Gehrels, G.E., 2007a. Lower Cretaceous strata in the Lhasa Terrane, Tibet, with implications for understanding the early tectonic history of the Tibetan Plateau. J. Sediment. Res. 77, 809–825.

Leier, A.L., DeCelles, P.G., Kapp, P., Ding, L., 2007b. The Takena Formation of the Lhasa terrane, southern Tibet: the record of a Late Cretaceous retroarc foreland basin. Geol. Soc. Am. Bull. 119, 31–48.

Leier, A.L., DeCelles, P.G., Kapp, P., Gehrels, G.E., Ding, L., 2007c. Detrital zircon geochronology of Phanerozoic sedimentary strata in the Lhasa terrane and implications for the tectonic evolution of southern Tibet. Basin Res. 19, 361–378.

Liu, D.Z., Tao, X.F., Ma, R.Z., Shi, H., Zhu, L.D., Hu, X.W., 2004. 1:250, 000 Geological Report of Coqen County with Geological Map. Chengdu University of Technology, Chengdu, pp. 163–183 (published in Chinese).

Liu, Q., Jiang, W., Jian, P., Ye, P.S., Wu, Z.H., Hu, D.G., 2006. Zircon shrimp U-Pb age and petrochemical and geochemical features of Mesozoic muscovite monzonitic granite at Ningzhong, Tibet. Acta Petrol. Sin. 22, 643–652.

Ludwig, K.R., 2001. Isoplot/Ex (Rev. 2.49): a Geochronological Toolkit for Microsoft Excel. 1. Berkeley Geochronology Center, Special Publication, pp. 1–58.

Mack, G.H., James, W.C., Monger, H.C., 1993. Classification of paleosols. Geol. Soc. Am. Bull. 105, 129–136.

Martina, F., Davila, F.M., Astini, R.A., 2006. Mio–Pliocene volcaniclastic deposits in the Famatina Ranges, southern Central Andes: a case of volcanic controls on sedimentation in broken foreland basins. Sediment. Geol. 186, 51–65.

Meng, F.Y., Zhao, Z.D., Zhu, D.C., Zhang, L.L., Guan, Q., Liu, M., Yu, F., Mo, X.X., 2010. Petrogenesis of Late Cretaceous adakite-like rocks in Mamba from the Eastern Gangdese, Tibet. Acta Petrol. Sin. 26, 2180–2192.

Miall, A.D., 1978. Facies types and vertical profile models in braided river deposits: a summary. In: Miall, A.D. (Ed.), Fluvial Sedimentology. Vol. 5. Canadian Society of Petroleum Geologists, Memoir, pp. 597–604.

Miall, A.D., 1996. The Geology of Fluvial Deposits: Sedimentary Facies, Basin Analysis, and Petroleum Geology. Springer Publishing, New York (pp, 582).

Mo, X.X., Hou, Z.Q., Niu, Y.L., Dong, G.C., Qu, X.M., Zhao, Z.D., Yang, Z.M., 2007. Mantle contributions to crustal thickening during continental collision: evidence from Cenozoic igneous rocks in southern Tibet. Lithos 96, 225–242.

Mo, X.X., Niu, Y.L., Dong, G.C., Zhao, Z.D., Hou, Z.Q., Zhou, S., Ke, S., 2008. Contribution of syncollisional felsic magmatism to continental crust growth: a case study of the Paleogene Linzizong Volcanic Succession in southern Tibet. Chem. Geol. 250, 49–67.

Murphy, M.A., Yin, A., Harrison, T.M., Dürr, S.B., Chen, Z., Ryerson, F.J., Kidd, W.S.F., Wang, X., Zhou, X., 1997. Did the Indo-Asian collision alone create the Tibetan plateau? Geology 25, 719–722.

Myrow, P.M., Southard, J.B., 1991. Combined-flow model for vertical stratification sequences in shallow marine storm-deposited beds. J. Sediment. Res. 61, 202–210.

Orme, D.A., Laskowaki, A.K., 2016. Basin analysis of the Albian–Santonian Xigaze forearc, Lazi Region, South-Central Tibet. J. Sediment. Res. 86, 894–913.

Orme, D.A., Carrapa, B., Kapp, P., 2014. Sedimentology, provenance and geochronology of the upper Cretaceous-lower Eocenewestern Xigaze forearc basin, southernTibet. Basin Res. 1–25.

Orton, G.J., Reading, H.G., 1993. Variability of deltaic processes in terms of sediment supply, with particular emphasis on grain size. Sedimentology 40, 475–512.

Pan, G.T., Ding, J., Yao, D.S., Wang, L.Q., 2004. Guide Book of 1:1,500,000 Geologic Map of the Qinghai-Xizang (Tibet) Plateau and Adjacent Areas. Cartographic Publishing House, Chengdu, China, pp. 1–148.

Posamentier, H.W., Allen, G.P., 1999. Siliciclastic sequence stratigraphy: concepts and applications. SEPM, Concepts in Sedimentology and Paleontology. Vol. 7 (pp. 210).

Reiss, Z., Hottinger, L., 1984. The Gulf of Aqaba, Ecological Micropaleontology, Ecological Studies. Springer-Verlag, Berlin Heidelberg New York Tokyo, pp. 1–354.

Searle, M.P., Windley, B.F., Coward, M.P., Cooper, D.J.W., Rex, A.J., Rex, D.C., Li, T.D., Xiao, X.C., Jan, Q., Thakur, V., Kumar, S., 1987. The closing of Tethys and the tectonics of the Himalaya. Geol. Soc. Am. Bull. 98, 678–701.

Soderlund, U., Patchett, P.J., Vervoort, J.D., Isachsen, C.E., 2004. The ^{176}Lu decay constant determined by Lu–Hf and U–Pb isotope systematics of Precambrian mafic intrusions. Earth Planet. Sci. Lett. 219, 311–324.

Sun, G.Y., Hu, X.M., Sinclair, H.D., Marcelle, B.K., Wang, J.G., 2015. Late Cretaceous evolution of the Coqen Basin (Lhasa terrane) and implications for early topographic growth on the Tibetan Plateau. Geol. Soc. Am. Bull. 127, 1001–1020.

Van Achterbergh, E., Ryan, C.G., Jackson, S.E., Griffin, W.L., 2001. Data reduction software for LA-ICPMS: appendix. Laser ablation-ICP-mass spectrometry in the earth sciences: principles and applications. Short Course Series. Vol. 29. Mineralog. Assoc. Canada, Ottawa, Ontario, pp. 239–243.

Van Wagoner, J.C., Posamentier, H.W., Mitchum, R.M., Vail, P.R., Sarg, J.F., Loutit, T.S., Hardenbol, J., 1988. An overview of sequence stratigraphy and key definitions. In: Wilgus, C.K., Hastings, B.S., Kendall, C.G.St.C., Posamentier, H.W., Ross, C.A., Van Wagoner, J.C. (Eds.), Sea-level Changes: AN Integrated Approach. Vol. 42. SEPM, Special Publication, pp. 39–45.

Van Wagoner, J.C., Mitchum, R.M., Campion, K.M., Rahmanian, V.D., 1990. Siliciclastic Sequence Stratigraphy in Well Logs, Cores, and Outcrops. American Association of Petroleum Geologists (Methods in Exploration Series 7: pp, 55).

Volkmer, J.E., Kapp, P., Guynn, J.H., Lai, Q., 2007. Cretaceous-Tertiary structural evolution of the north central Lhasa terrane, Tibet. Tectonics 26, TC6007. http://dx.doi.org/10.1029/2005TC001832.

Walker, R.G., Plint, A.G., 1992. Wave- and storm-dominated shallow marine systems. In: Walker, R.G., James, N.P. (Eds.), Facies Models; Response to Sea Level Change. Geological Association of Canada, pp. 219–238.

Wang, C., Liu, Z., 1999. Xigaze Forearc Basin and Yarlung Zangbo Suture Zone, Tibet (in Chinese). Geological Publishing House, Beijing (pp, 237).

Wang, C., Li, X., Liu, Z., Li, Y., Jansa, L., Dai, J., Wei, Y., 2012. Revision of the Cretaceous-Paleogene stratigraphic framework, facies architecture and provenance of the Xigaze forearc basin along the Yarlung Zangbo suture zone. Gondwana Res. 22, 415–433.

Wang, J.G., Hu, X.M., Garzanti, E., An, W., Liu, X.C., 2017. The birth of the Xigaze forearc basin in southern Tibet. Earth Planet. Sci. Lett. 465, 38–47.

Weislogel, A.L., Graham, S.A., Chang, E.Z., Wooden, J.L., Gehrels, G.E., Yang, H.S., 2006. Detrital zircon provenance of the Late Triassic Songpan-Ganzi complex: sedimentary record of collision of the North and South China blocks. Geology 34, 97–100.

Wen, D.R., Liu, D.Y., Chung, S.L., Chu, M.F., Ji, J.Q., Zhang, Q., Song, B., Lee, T.Y., Yeh, M.W., Lo, C.H., 2008. Zircon SHRIMP U-Pb ages of the Gangdese Batholith and implications for Neotethyan subduction in southern Tibet. Chem. Geol. 252, 191–201.

Wray, J.L., 1977. Calcareous algae. Developments in Palaeontology and Stratigraphy, Vol IV. Elsevier, Amsterdam, pp. 1–185.

Wu, F.Y., Ji, W.Q., Liu, C.Z., Chung, S.L., 2010. Detrital zircon U-Pb and Hf isotopic data from the Xigaze forearc basin: constraints on Transhimalayan magmatic evolution in southern Tibet. Chem. Geol. 271, 13–25.

Xie, Y.W., Peng, X.J., Xiluo, L., 2007. 1:250,000 Geological Report of Lhasa and Zedong Area with Geological Maps (in Chinese) (pp, 315).

Xu, R.H., Schärer, U., Allègre, C.J., 1985. Magmatism and metamorphism in the Lhasa block (Tibet): a geochronological study. J. Geol. 93, 41–57.

Yin, A., Harrison, T.M., 2000. Geologic evolution of the Himalayan-Tibetan orogen. Annu. Rev. Earth Planet. Sci. 28, 211–280.

Yin, J., Xu, J., Liu, C., Li, H., 1988. The Tibetan Plateau: regional stratigraphic context and previous work. Philos. Trans. R. Soc. Lond. 327, 5–52 series A.

Zhang, K.J., 2000. Cretaceous paleogeography of Tibet and adjacent areas (China): tectonic implications. Cretac. Res. 21, 23–33.

Zhang, K.J., Xia, B.D., Wang, G.M., Li, Y.T., Ye, H.F., 2004. Early Cretaceous stratigraphy, depositional environments, sandstone provenance, and tectonic setting of central Tibet, western China. Geol. Soc. Am. Bull. 116, 1202–1222.

Zhang, H.F., Xu, W.C., Guo, K.Q., Cai, H.M., Yuan, H.L., 2007a. Zircon U-Pb and Hf isotopic composition of deformed granite in the southern margin of the Gangdese Belt, Tibet: evidence for Early Jurassic subduction of neo-tethyan oceanic slab. Acta Petrol. Sin. 23, 1347–1353 (in Chinese with English abstract).

Zhang, H.F., Xu, W.C., Guo, J.Q., Zong, K.Q., Cai, H.M., Yuan, H.L., 2007b. Indosinian orogenesis of the Gangdese terrane: evidences from zircon U-Pb dating and petrogenesis of granitoids. Earth Sci. 32, 155–166 (in Chinese with English abstract).

Zhang, Q., Ding, L., Cai, F., Xu, X., Zhang, L., Xu, Q., Willems, H., 2011. Early Cretaceous Gangdese retroarc foreland basin evolution in the Selin Co Basin, central Tibet. Evidence from Sedimentology and Detrital Zircon Geochronology. 353. Geological Society, London, Special Publications, pp. 27–44.

Zhang, K.J., Zhang, Y., Tang, X., Xia, B., 2012. Late Mesozoic tectonic evolution and growth of the Tibetan plateau prior to the Indo-Asian collision. Earth Sci. Rev. 114, 236–249.

Zhou, C.Y., Zhu, D.C., Zhao, Z.D., Xu, J.F., Wang, L.Q., Chen, H.H., Xie, L.W., Dong, G.C., Zhou, S., 2008. Petrogenesis of Daxiong pluton in western Gangdese, Tibet: Zircon U-Pb dating and Hf isotopic constraints. Acta Petrol. Sin. 24, 348–358 (in Chinese with English abstract).

Zhu, D.C., Mo, X.X., Zhao, Z.D., Xu, J.F., Zhou, C.Y., Sun, C.G., Wang, L.Q., Chen, H.H., Dong, G.C., Zhou, S., 2008. Zircon U-Pb geochronology of Zenong Group volcanic rocks in Coqen area of Gangdese, Tibet and tectonic significance. Acta Petrol. Sin. 24, 401–412 (in Chinese with English abstract).

Zhu, D.C., Mo, X.X., Niu, Y.L., Zhao, Z.D., Wang, L.Q., Liu, Y.S., Wu, F.Y., 2009. Geochemical investigation of Early Cretaceous igneous rocks along an east-west traverse throughout the central Lhasa Terrane, Tibet. Chem. Geol. 268, 298–312.

Please cite this article as: Sun, G., et al., Early Cretaceous palaeogeographic evolution of the Coqen Basin in the Lhasa Terrane, southern Tibetan Plateau, Palaeogeogr. Palaeoclimatol. Palaeoecol. (2017), http://dx.doi.org/10.1016/j.palaeo.2017.06.006

Zhu, D.C., Zhao, Z.D., Niu, Y.L., Mo, X.X., Chung, S.L., Hou, Z.Q., Wang, L.Q., Wu, F.Y., 2011a. The Lhasa Terrane: record of a microcontinent and its histories of drift and growth. Earth Planet. Sci. Lett. 301, 241–255.

Zhu, D.C., Zhao, Z.D., Niu, Y.L., Dilek, Y., Mo, X.X., 2011b. Lhasa terrane in southern Tibet came from Australia. Geology 39, 727–730.

Zhu, D.C., Zhao, Z.D., Niu, Y.L., Dilek, Y., Hou, Z.Q., Mo, X.X., 2013. The origin and pre-Cenozoic evolution of the Tibetan Plateau. Gondwana Res. 23, 1429–1454.

Zhu, D.C., Wang, Q., Zhao, Z.D., Chung, S.L., Cawood, P.A., Niu, Y.L., Liu, S.A., Wu, F.Y., Mo, X.X., 2015. Magmatic record of India-Asia collision. Sci Rep 5:14289. http://dx.doi.org/10.1038/srep14289.

Zhu, D.C., Li, S.M., Cawood, P.A., Wang, Q., Zhao, Z.D., Liu, S.A., Wang, L.Q., 2016. Assembly of the Lhasa and Qiangtang terranes in central Tibet by divergent double subduction. Lithos 245, 7–17.

Please cite this article as: Sun, G., et al., Early Cretaceous palaeogeographic evolution of the Coqen Basin in the Lhasa Terrane, southern Tibetan Plateau, Palaeogeogr. Palaeoclimatol. Palaeoecol. (2017), http://dx.doi.org/10.1016/j.palaeo.2017.06.006